AD-A040 934 TEXAS UNIV AT DALLAS RICHARDSON F/G 4/1
AURORAL DATA ANALYSIS,(U)
FEB 77 J D WINNINGHAM, W J HEIKKILA F19628-76-C-0005
UNCLASSIFIED SCIENTIFIC-1 AFGL-TR-77-0047 NL

| OF |
AD
A040 934

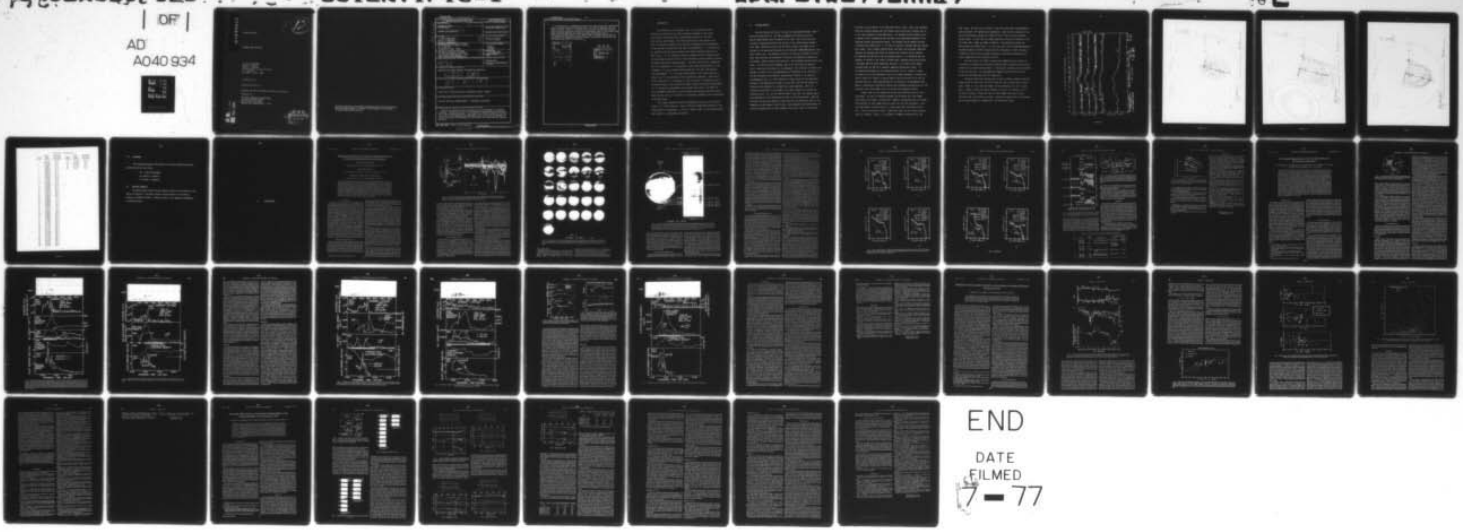

END
DATE
FILMED
7-77

AFGL-TR-77-0047

AURORAL DATA ANALYSIS

J. David Winningham
Walter J. Heikkila
Gordon G. Shepherd
The University of Texas at Dallas
P. O. Box 688
Richardson, Texas 75080

15 February 1977

Scientific Report No. 1

Prepared for

AIR FORCE GEOPHYSICS LABORATORIES
AIR FORCE SYSTEMS COMMAND
UNITED STATES AIR FORCE
HANSCOM AFB, MASSACHUSETTS 07131

SECURITY CLASSIFICATION OF THIS PAGE (When Data Entered)

(19) REPORT DOCUMENTATION PAGE		READ INSTRUCTIONS BEFORE COMPLETING FORM
(18) 1. REPORT NUMBER AFGL-TR-77-0047	2. GOVT ACCESSION NO.	3. RECIPIENT'S CATALOG NUMBER
(6) 4. TITLE (and Subtitle) AURORAL DATA ANALYSIS		5. TYPE OF REPORT & PERIOD COVERED Scientific Report No.1
		6. PERFORMING ORG. REPORT NUMBER
(10) 7. AUTHOR(s) J. David Winningham, Walter J. Heikkila, Gordon G. Shepherd *		(15) 8. CONTRACT OR GRANT NUMBER(s) F19628-76-C-0005
9. PERFORMING ORGANIZATION NAME AND ADDRESS The University of Texas at Dallas P. O. Box 688 Richardson, Texas 75080		10. PROGRAM ELEMENT, PROJECT, TASK AREA & WORK UNIT NUMBERS 62101F 76630801
11. CONTROLLING OFFICE NAME AND ADDRESS Air Force Geophysics Laboratory Hanscom AFB, Massachusetts 01731 Capt. Edward Weber/PHI/Monitor		(11) 12. REPORT DATE 15 February 1977
		13. NUMBER OF PAGES 47
14. MONITORING AGENCY NAME & ADDRESS (if different from Controlling Office) (12) 48 p.		15. SECURITY CLASS. (of this report) Unclassified
		15a. DECLASSIFICATION/DOWNGRADING SCHEDULE

16. DISTRIBUTION STATEMENT (of this Report)

Approved for Public Release: Distribution Unlimited

(16) 7663 (17) 98

17. DISTRIBUTION STATEMENT (of the abstract entered in Block 20, if different from Report)

(17) Scientific-1

18. SUPPLEMENTARY NOTES

*York Univ. 4700 Keele Street, Downsview, Ontario, Canada

19. KEY WORDS (Continue on reverse side if necessary and identify by block number)

Auroral Particles, Magnetosphere - Ionosphere Interaction

20. ABSTRACT (Continue on reverse side if necessary and identify by block number)

During the previous year four papers have been published in refereed journals. In addition one more is accepted for publication and three more are in the refereeing process. Each deals with effects produced by auroral particles on the ionosphere and atmosphere and in turn how the dynamics of auroral particles are influenced by terrestrial and interplanetary magnetic activity.

→ next page

DD FORM 1 JAN 73 1473 EDITION OF 1 NOV 65 IS OBSOLETE

391647

Unclassified

SECURITY CLASSIFICATION OF THIS PAGE (When Data Entered)

1/2

cont

In particular, a framework has been laid that relates the equatorward edge of auroral particle precipitation to the IMF B_z component and substorm activity. Work is at present being carried on that both qualitatively and quantitatively relates the equatorward edge of the trough to the 6300 A optical emission and electron fluxes observed by ISIS 2. Utilizing electron fluxes as the common link, is hoped that the end result will be an empirical relation between the poleward trough wall and influences what modify its position.

I. INTRODUCTION

The objectives of this contract are: (1) to relate the 6300 A emissions as observed by the ISIS-2 scanning photometer to the causative electron fluxes which are simultaneously observed by the ISIS-2 Soft Particle Spectrometer. The energy sub-region of the electron flux which is primarily responsible for the 6300 A emissions will be delineated to the accuracy available with the ISIS-2 instrumentation. It is hoped that an empirical relation can be derived that relates electron energy flux to 6300 A flux. (2) To compare the particle fluxes and 6300 A emissions (and the conclusions derived in Item 1) with simultaneous electron density profiles obtained by the ISIS-2 topside sounder. The basic goal of such a comparison will be to ascertain if it is possible to infer gross characteristics of the ionosphere (e.g. f_oF_2, plasma trough boundaries) from 6300 A and particle flux measurements. (3) To relate, where possible, the results obtained in items 1 and 2 to the dynamical effects produced by substorms. Specifically we will evaluate if it is possible to infer the motion of boundaries such as the poleward edge of the low-altitude plasma trough from indirect measurements. (4) To analyze the simultaneous data obtained with ISIS-2, the AFCRL Airborne Ionospheric Laboratory, and the Defense Meterological Satellite System. Again the goal will be to ascertain if ionospheric parameters can be determined by indirect means.

This report represents the work accomplished during the first twelve months of a 39 month contract. Most of the work accomplished during the first twelve months was preparatory in nature. However, item 3 of the objectives has been brought to a reasonable conclusion.

II. ACCOMPLISHMENTS

The work dealing with item 3 relates the equatorward boundary >100 eV electron precipitation to the IMF B_z component and substorm activity. Electron spectrograms from 351 passes of the ISIS 1 and 2 satellites were utilized to study statistically the effects of the interplanetary magnetic field (IMF), substorm activity, and the earth's dipole tilt angle on the latitude of the equatorward boundary of the nightside (2000-0400 magnetic local time) auroral oval. The boundary location (in invariant latitude) at hourly local time intervals was identified in terms of the equatorward boundary of the diffuse, >100 eV electron precipitation. The following characteristics were noted: (1) The north-south component (B_z) of the IMF plays the dominant role in controlling the motion of this boundary. The invariant latitude of the boundary is shown to shift by approximately 4^o depending on the direction of the IMF (northward and southward, respectively) relative to its position corresponding to $B_z = 0$. This indicates an inward motion of the associated boundary in the magnetotail by about 5 earth radii when the IMF changes its direction from northward to southward with large magnitude. There is a significant difference in the amount of the shift between the evening and morning sectors, i.e., for the same decrease in B_z value, the boundary moves more equatorward in the morning sector than in the evening sector. When the obtained oval particle boundary is projected onto the equatorial plane of the magnetotail along magnetic field lines, a good agreement was found between the projected boundary and the drift boundary (the Alfven layer) of low energy

electrons in the presence of the dawn-dusk electric field. Thus, this agreement gives new evidence showing that the diffuse auroral particles originate near or at the inner boundary of the plasma sheet. (2) Substorm activity seems to have a separate role in determining the latitude of the equatorward boundary of the nightside auroral precipitation region. The boundary during substorm periods is statistically found to be 2 - 3^{o} lower in invariant latitude than that during quiet times. Even a simple classification into quiet and disturbed conditions improves the accuracy with which the auroral oval location can be inferred. By combining the IMF effect and the substorm effect, it is indicated that the boundary is located at the lowest latitudes when a substorm takes place during a southward IMF with large magnitude, whereas it is located in the highest latitudes when the IMF has a northward component during quiet times. (3) The equatorward boundary of the nightside auroral oval is located in higher latitudes in the winter hemisphere than in the summer hemisphere, although this earth's dipole tilt effect is usually smaller than the effects of the IMF and substorm activity. These phenomenalogical relationships, in conjunction with papers in preparation relating the optical and ionospheric manifestation of >100 electrons, will allow items 1 and 2 to be tied into dynamical effects.

Items 1 and 2 of the objectives involve data from more than one ISIS 2 instrument. In order to adequately compare the different data sets common data formats are needed. In particular, computer manipulable media are needed. Unfortunately, no such common data set exists for any ISIS instruments. Each ISIS experimenter received digital or analog tapes which contained only his data. Thus we have had to create a common data base. We have chosen magnetic tapes as a medium. Figure 1 is an example of computer merged particle and

6300 A data. The top trace of Figure 1 gives the pitch angle corresponding to each measurement (0^{o} represents precipitation). The next four panels give the electron directional energy flux (ergs cm^{-2} $ster^{-1}$ sec) for four selectable energy ranges. In this case the energy ranges are, from top to bottom 0 to 60 60 to 300, 300 to 1000, and 1000 to 15000 eV. The bottom trace gives the narrow band (10 A) 6300 A data. It can be seen that there is good morphological agreement between the 6300 A emission and the low-energy (<1 keV) electrons. It should be noted that this format represents a quick-look presentation for visual inspection of the collective data set.

The next step in the 6300 A electron flux comparison will involve the derivation of an empirical relationship between 6300 A intensities and electron energy flux in selected energy bands. A multivariate analysis will be performed on the two data sets. The aforementioned computer generated plots will be utilized in selecting data sets for comparison.

During the past year programs were written to produce computer generated contour plots of 6300, 5577, and 3914 A from the ISIS 2 scanner data on microfilm. Figure 2 a to d shows an example of the presentation for ISIS 2 orbit 13101. Figure 2a shows the 6300 A contours, 2b the 5577 A contours, and 2c the 3914 A contours. Figure 2d lists the spin number from start of data, universal time, and invariant latitude. Ninety-five passes have been processed and are being readied for submission to the World Data Center.

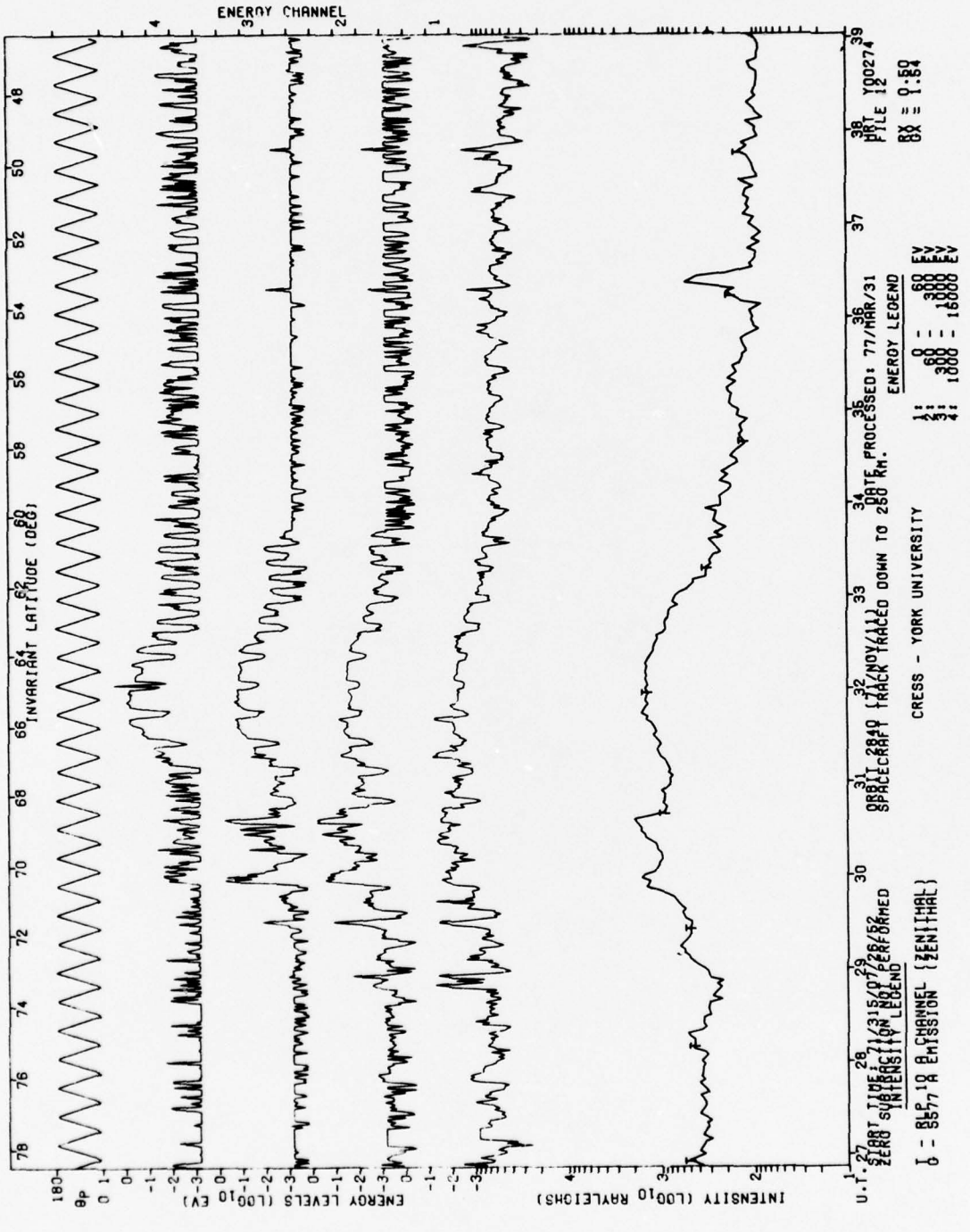
ISIS-II SPACECRAFT TRACK - PHOTOMETRIC EMISSION RATES
ENERGY CHANNEL
INVARIANT LATITUDE (DEG)
ENERGY LEVELS (LOG10 EV)
INTENSITY (LOG10 RAYLEIGHS)
U.T.
START TIME 71/315/07:29:26/52
ZERO SUBTRACTION NOT PERFORMED
INTENSITY LEGEND
δ - BLP 10 A CHANNEL (ZENITHAL)
5577 A EMISSION (ZENITHAL)
ORBIT 2849 (71/NOV/11)
SPACECRAFT TRACK TRACED DOWN TO 260 Km.
DATE PROCESSED: 77/MAR/31
ENERGY LEGEND
1: 0 - 60 EV
2: 60 - 300 EV
3: 300 - 1000 EV
4: 1000 - 10000 EV
CRESS - YORK UNIVERSITY
ART FILE 12 Y00274
BX = 0.69

Figure 1

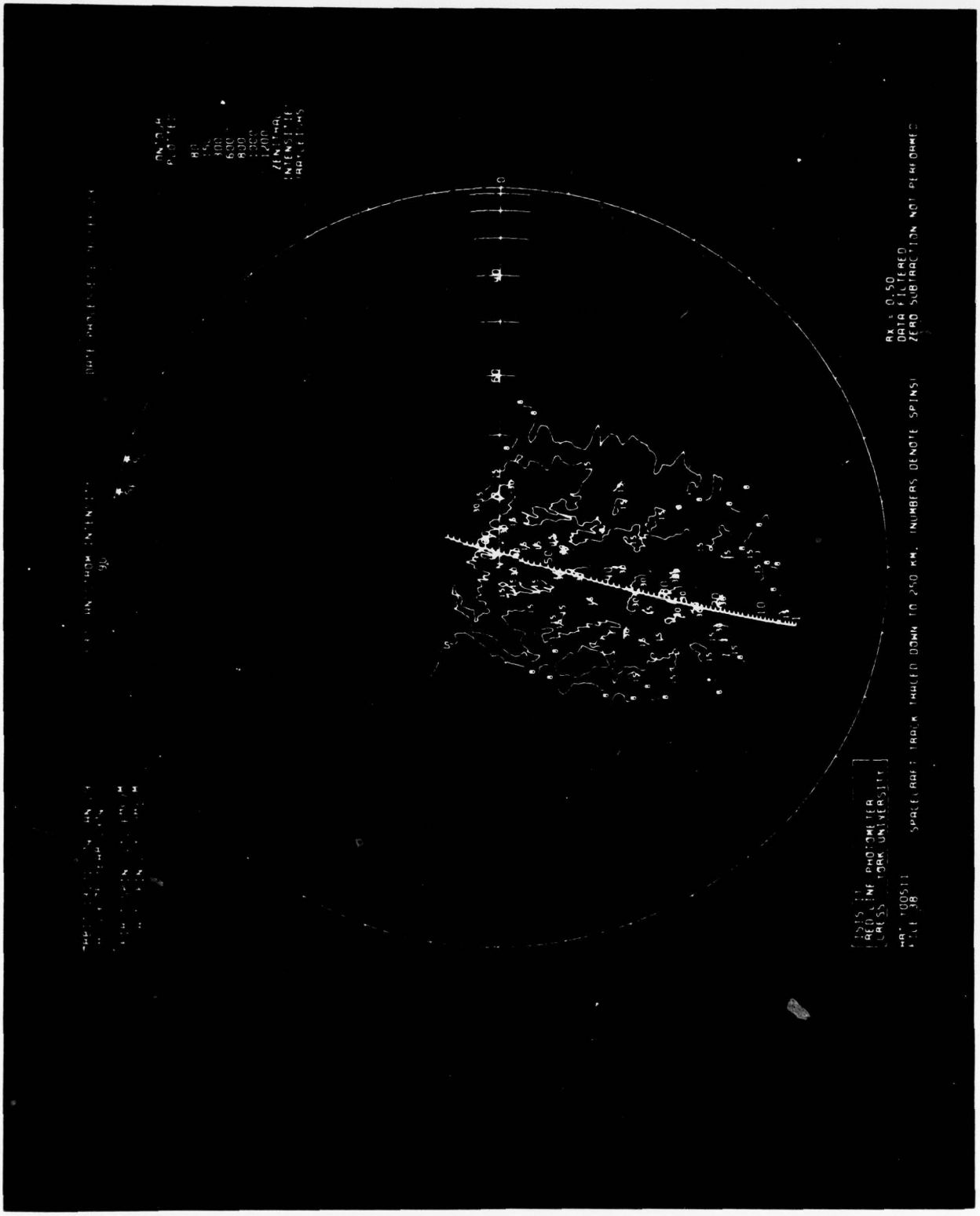
Rx = 0.50
DATA FILTERED
ZERO SUBTRACTION NOT PERFORMED
SPACECRAFT TRACK TRAILED DOWN TO 250 KM. (NUMBERS DENOTE SPINS)

Figure 2a

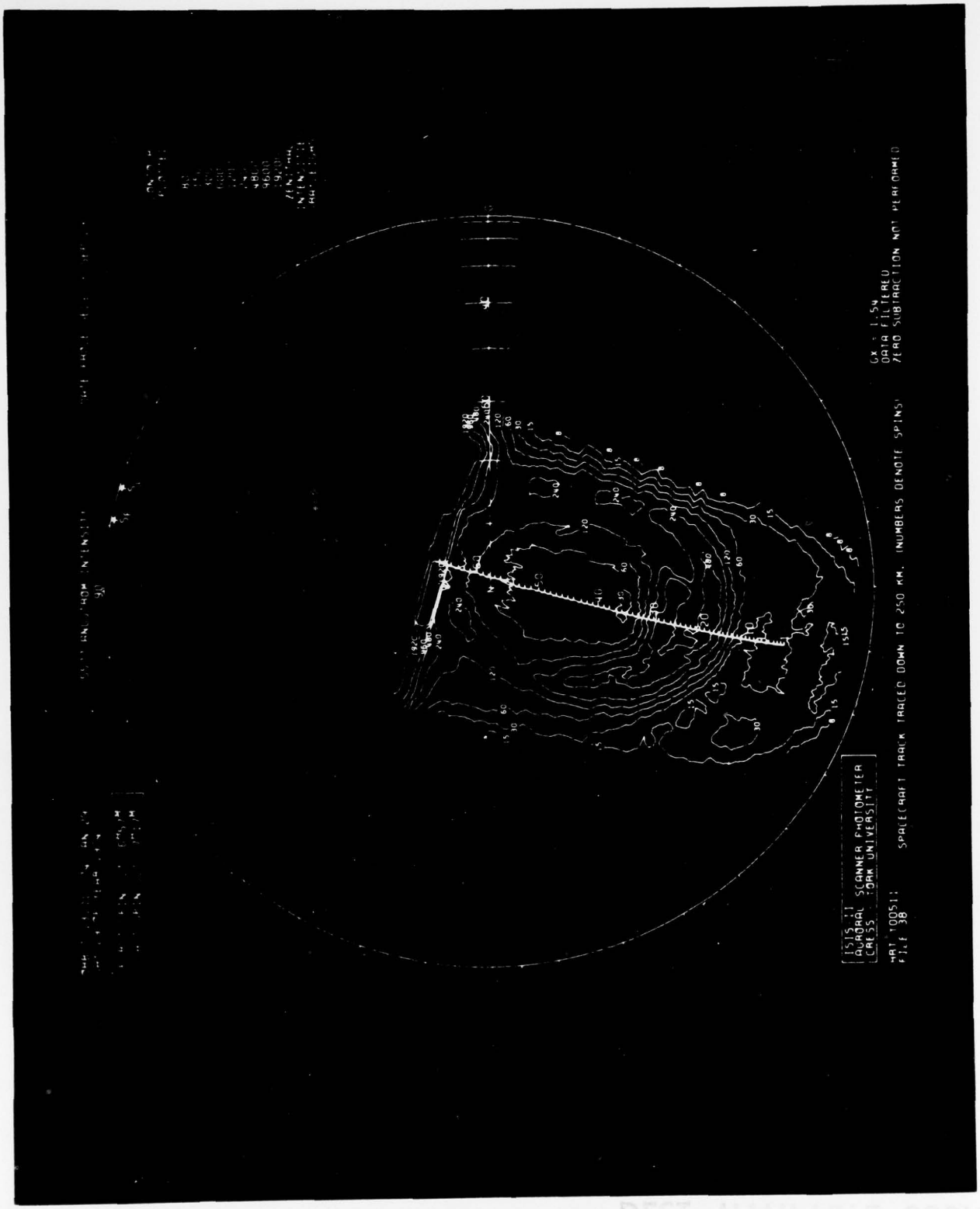

Figure 2b

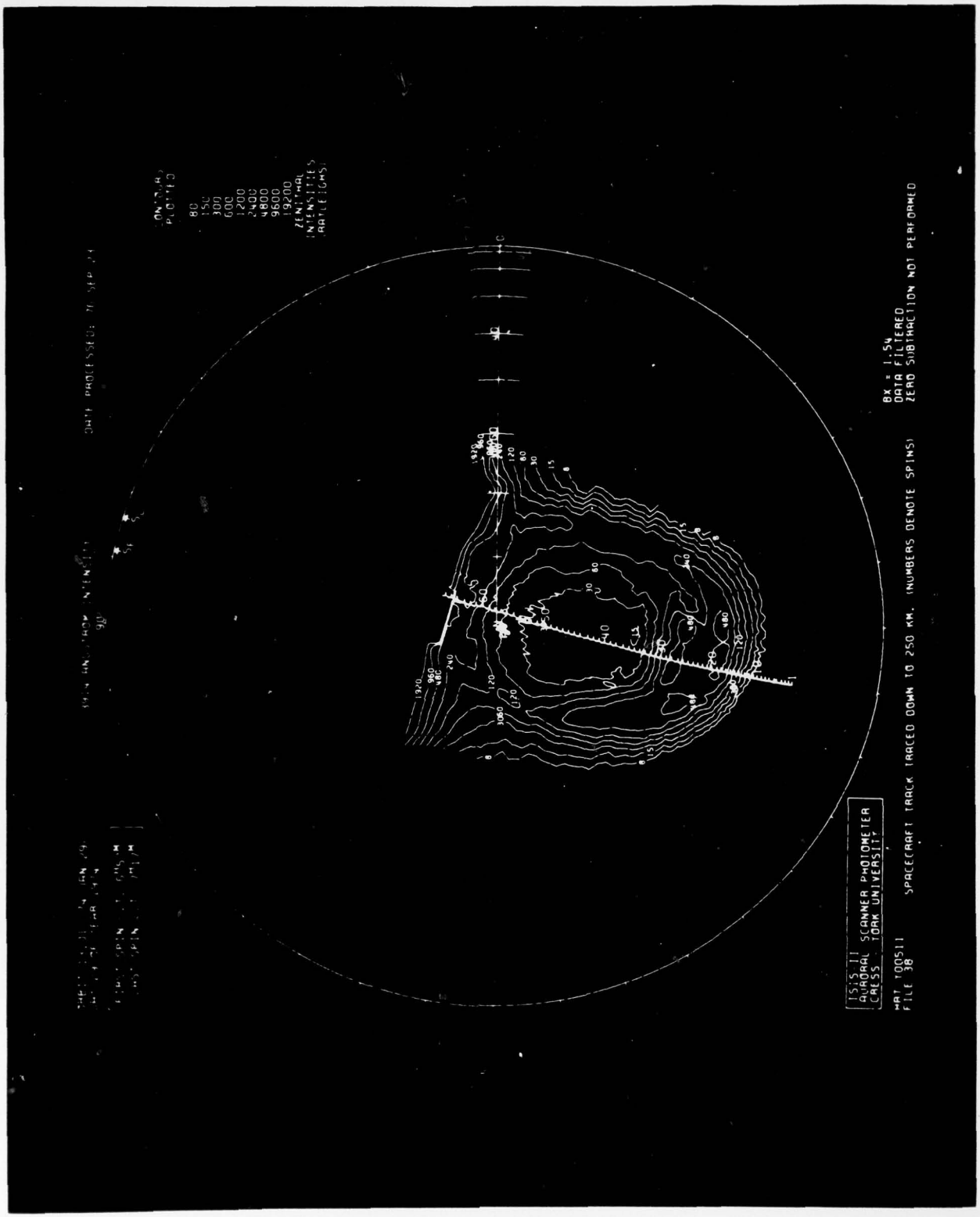

Figure 2c

SPACECRAFT INFORMATION

SPIN NUMBER	ORBIT TIME (HRMNSC)	INVARIANT LATITUDE (DEGREES)	SPIN NUMBER	ORBIT TIME (HRMNSC)	INVARIANT LATITUDE (DEGREES)
1	065724	49.3	61	071605	79.3
2	065742	50.1	62	071623	78.6
3	065760	50.9	63	071641	77.8
4	065818	51.7	64	071705	76.7
5	065842	52.8	65	071723	75.9
6	065854	53.3	66	071741	75.2
7	065918	54.4			
8	065936	55.3			
9	065954	56.1			
10	070012	56.9			
11	070030	57.8			
12	070048	58.6			
13	070106	59.4			
14	070130	60.5			
15	070148	61.4			
16	070206	62.2			
17	070224	63.0			
18	070242	63.9			
19	070260	64.7			
20	070318	65.5			
21	070336	66.4			
22	070354	67.2			
23	070412	68.0			
24	070430	68.9			
25	070448	69.7			
26	070506	70.5			
27	070524	71.3			
28	070548	72.4			
29	070606	73.2			
30	070624	74.1			
31	070642	74.9			
32	070659	75.7			
33	070717	76.5			
34	070735	77.3			
35	070753	78.1			
36	070811	78.8			
37	070829	79.5			
38	070853	80.6			
39	070911	81.6			
40	070929	82.5			
41	070947	83.2			
42	071005	83.6			
43	071023	83.9			
44	071047	84.2			
45	071105	84.3			
46	071123	84.3			
47	071141	84.3			
48	071159	84.3			
49	071217	84.2			
50	071235	84.2			
51	071259	84.3			
52	071317	84.3			
53	071335	84.4			
54	071353	84.3			
55	071411	84.1			
56	071429	83.5			
57	071447	82.7			
58	071511	81.6			
59	071529	80.8			
60	071547	80.1			

Figure 2d

III. PERSONNEL

The following personnel contributed to the work performed during the period covered by this report,

Dr. J. David Winningham

Dr. Walter J. Heikkila

Dr. Gordon G. Shepherd

IV. RELATED CONTRACTS

All publications covered by this specific contract are attached to this report as section V. The most relevant related contract to the present contract is F19628-75-C-0032. F19628-75-C-0032 is the immediate predecessor to F19628-76-C-005.

V. PUBLICATIONS

VOL. 81, NO. 31 JOURNAL OF GEOPHYSICAL RESEARCH NOVEMBER 1, 1976

Simultaneous Observations of Discrete and Diffuse Auroras by the Isis 2 Satellite and Airborne Instruments

CHARLES STERLING DEEHR

Geophysical Institute, University of Alaska, Fairbanks, Alaska 99701

J. DAVID WINNINGHAM

Center for Space Studies, University of Texas at Dallas, Richardson, Texas 75082

FUMIHIKO YASUHARA AND SYUN-ICHI AKASOFU

Geophysical Institute, University of Alaska, Fairbanks, Alaska 99701

All-sky camera and photometric data were obtained by airborne instrumentation as a function of latitude and time during the course of an auroral substorm. During the substorm recovery phase the Isis 2 satellite passed within 60 km of the aircraft zenith. The discrete and diffuse auroral regions were identified from the airborne all-sky camera data. Satellite and photometric observations of the corresponding incoming particles led to the following conclusions: (1) The diffuse and the discrete auroras seen in the all-sky camera data correspond to the two different particle precipitation regions observed from satellites and referred to as CPS and BPS, respectively (Winningham et al., 1975). (2) The diffuse auroral region is associated with high-energy stably trapped energetic electrons, and the discrete aurora is poleward of the stable electron trapping boundary. (3) The latitudinal distribution of characteristic particle energies does not change in a relative sense during the poleward expansion, but expands 'accordionlike.' (4) The height-integrated intensity ratio of the red (6300 Å) to green (5577 Å) emissions of atomic oxygen is a good indicator of the characteristic energy of the incoming particle spectrum.

INTRODUCTION

The auroral scanners aboard the Isis 2 and DMSP satellites have identified at least two types of auroras, the discrete and diffuse auroras [*Lui and Anger*, 1973; *Snyder et al.*, 1974; *Lui et al.*, 1975]. It is thus of great interest to examine the corresponding features in the pattern of precipitation of auroral particles. The precipitation patterns of auroral electrons along magnetic meridian lines have been studied by *Frank and Ackerson* [1971], *Hoffman and Burch* [1973], *Deehr et al.* [1973], and most recently by *Winningham et al.* [1975]. In general, the latitudinal profiles have suggested that one can distinguish at least two precipitation regions. Winningham et al. refer to these as the BPS (boundary plasma sheet) and CPS (central plasma sheet) regions, corresponding to the regions of discrete and diffuse auroras, respectively. The 'inverted V' structure [*Frank and Ackerson*, 1971] and 'lambda structures' [*Sharber and Heikkila*, 1972] are usually embedded in the BPS region.

In order to examine relationships between the precipitation pattern of auroral electrons and the two auroral regions a simultaneous observation, from above by the Isis 2 satellite and from below by the NASA 711 jet aircraft, was conducted over the Arctic Ocean on October 10, 1972. The purpose of this paper is to report some of the results of these observations.

OBSERVATIONAL CIRCUMSTANCES

Figure 1 shows both the satellite trajectory and the aircraft path, together with the *AU* and *AL* indices during the period of interest. Instead of projecting the satellite trajectory radially down to the earth's surface, it is projected along the geomagnetic field lines, to an altitude of 110 km, at which most of the precipitating electrons of the observed average energy are stopped. Over the Arctic Ocean, off Barrow, the aircraft headed first in the antiparallel direction to the expected Isis 2 trajectory (0857–1030 UT) and then flew parallel to the trajectory between 1030 and 1110 UT. The satellite passed nearest to the aircraft between 1104 and 1105 UT.

The aurora was very quiet until about 0930 UT and became quite active afterwards (see Figure 2). Several surges were observed between 0930 and 1010 UT, and an intense poleward motion began at about 1020 UT. At that time the aircraft was flying poleward, but the auroral motion overtook the aircraft at about 1023 UT and went far poleward of it by 1030 UT, at which time the aircraft turned equatorward. The satellite passed the nearest point to the aircraft when the aircraft was located approximately on the boundary between the diffuse and discrete auroral regions (70.0°N geographic latitude, 166.0°W geographic longitude). This can be seen more clearly in the all-sky photograph shown on the left-hand side of Figure 3.

In the all-sky photograph (Figure 3) we can easily distinguish two types of aurora, i.e., the brighter aurora poleward of the aircraft and the other less bright aurora, equatorward of it. Although almost no structure can be seen in the poleward aurora (because of the saturation of the film), some folds or wavy shapes are apparent near the western horizon, indicating rayed structure. Thus it is reasonable to identify the poleward aurora as a discrete aurora; in fact, it was the arc which advanced poleward at about 1020 UT. On the other hand, the equatorward aurora has a much more uniform and diffuse luminosity and could therefore be identified as a diffuse aurora.

The satellite traversed the auroral region between 1103 and 1107 UT, which was during the recovery phase of the substorm (a 200-γ negative bay at College; see Figure 1, bold line). The satellite path (again projected along the geomagnetic field lines to an altitude of 110 km) is plotted every 10 s from 1103:20 to 1106:00 UT on the all-sky photograph (Figure 3). The circled

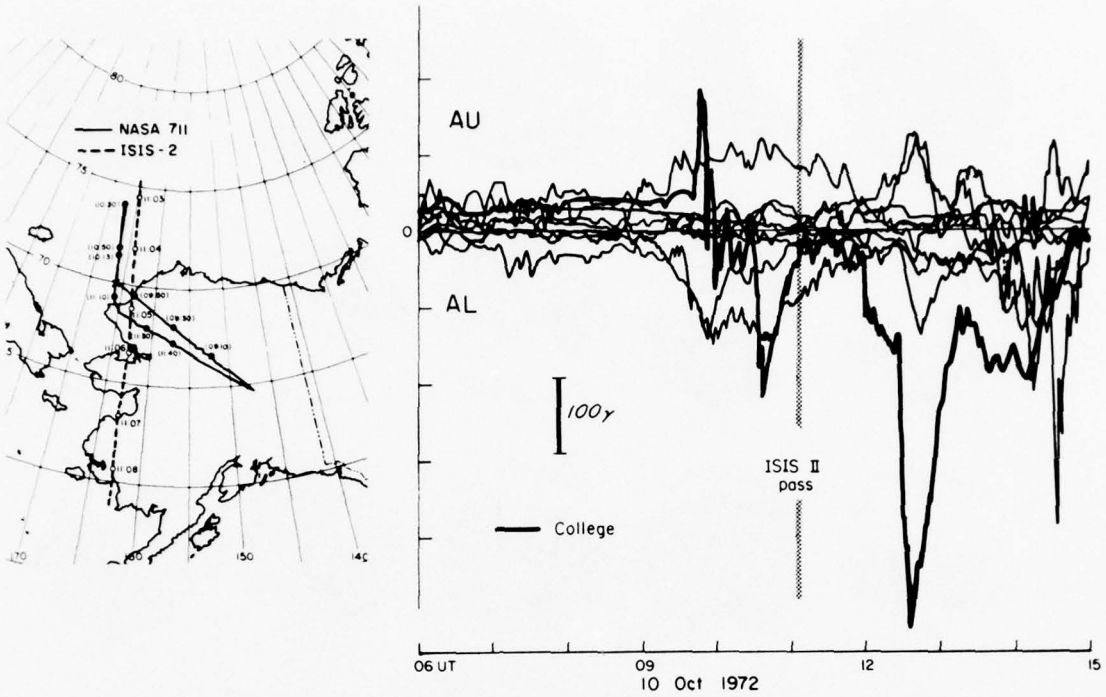

Fig. 1. A map of the Alaskan sector showing the route of the airplane (solid line) and that of the satellite (dashed line), labeled in universal time. Shown also are the *AU* and *AL* magnetic indices consisting of the envelope of auroral region *H* component magnetograms. The College magnetometer is shown as a heavier line.

dot indicates the point where the projected latitude of the satellite is 70.0°N, which is also the latitude of the zenith of the all-sky photograph. The longitudes of the zenith and the circled dot are different by approximately 60 km.

The soft particle spectrometer (SPS) spectrogram for this pass is shown on the right-hand side of Figure 3; for details of the spectrogram, see *Winningham et al.* [1975]. The satellite crossed the poleward edge of the auroral precipitation at 1103:31 UT and the equatorward edge at 1106:28 UT.

In the spectrogram we can also recognize two types of the particle precipitation, poleward and equatorward of approximately 70°N geographic latitude. The poleward precipitation shows a considerable structure and has an intense flux and higher average energy, while the equatorward one shows almost no structure (except for a very low energy burst around 1105:40 UT) and has a weaker flux and a lower average energy. Thus these two regions correspond to the BPS and CPS, respectively [*Winningham et al.*, 1975]. It can be seen that the aircraft was located near the boundary between the two precipitation regions during the satellite pass.

Satellite Observations

The low-energy (<15 keV) electron data obtained by Isis 2 (see Figure 3) can be regarded as a 'snapshot' of the late substorm electron latitudinal profile. As mentioned in the previous section, two distinctively different regions can be recognized in the spectrogram. From 1103:23 UT (Λ = 70.8°) to 1104:32 UT (Λ = 67.6°) a band of structured intense electron flux was observed. At lower latitudes from 1104:32 to 1106:28 UT (Λ = 62.3°) a relatively uniform weaker electron flux was measured. In Figures 4*a*–4*d*, spectra representative of the structured region are presented, as is done for the diffuse precipitation in Figures 4*e*–4*h*.

The energy spectrum of auroral primary electrons can often be described by an equation of a Maxwellian type: $N(E)\,dE = N_0 E \exp(-E/\alpha)$ el cm^{-2} s^{-1} eV^{-1}, where α ($= kT_e$) is the 'characteristic energy,' or the energy at the peak of the distribution. As can be seen in Figures 4*e*–4*h*, the high-energy end of the spectrum in the diffuse auroral region is well described by a Maxwellian distribution, but the low-energy portion is best described by a power law. An exception to the low-energy power law was observed in spectrum 4*g*. This spectrum was taken from the low-energy burst observed in the spectrogram (Figure 3) at approximately 1105:30 UT. The low-energy burst cannot be described by a Maxwellian distribution either, the observed spectrum being narrower than a Maxwellian. This low-energy burst constitutes only a minor fraction of the total energy flux and thus does not contribute significantly to the auroral luminosity.

The characteristic energy of the electron spectra in the diffuse zone gradually increased from 0.9 keV as the invariant latitude decreased. A maximum of 1 keV was reached at ~1105:50 UT (Λ = 63.9°) after which time it gradually decreased to 0.6 keV (Figures 4*e*–4*h*). The power law portion (at low energies) of the observed spectra could be due to conjugate degraded primaries and secondaries.

The structured auroral region exhibits a variety of spectra, some of which are described by a Maxwellian curve (Figures 4*a* and 4*d*) and others which are not (Figures 4*b* and 4*c*). Spectrum 4*a* was obtained in the region just poleward of the intense bursts. Spectra 4*b* and 4*c* were obtained in the region of intense bursts and highest average energy. Spectrum 4*d* was observed just equatorward of the most intense bursts and is Maxwellian in shape except for the low-energy region, which is power law. Its characteristic energy (1.4 keV) is higher and its total energy input is greater than those observed in the diffuse

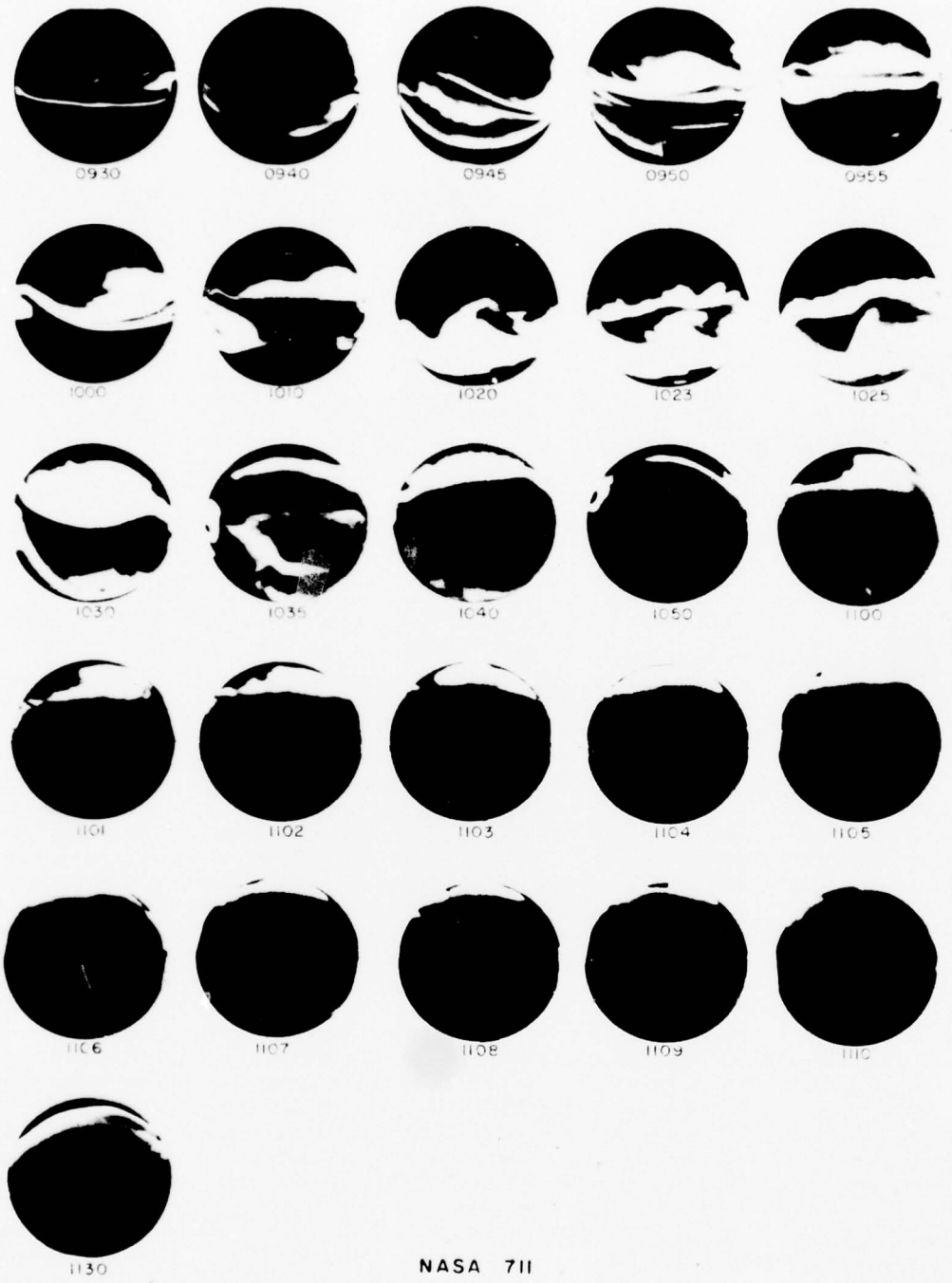

Fig. 2. A collection of all-sky camera photographs taken from the NASA 990 aircraft during the flight of October 10, 1972. The substorm begins over the aircraft at 0930 and expands poleward (up) with the aircraft until the aircraft turns equatorward at 1030, flying under the diffuse aurora to the end of the flight (geomagnetic north is up and east is to the right).

region (Figures 4*e*–4*h*).

The spectra shown in Figures 4*b* and 4*c* cannot be fitted with a Maxwellian distribution. These spectra can be better characterized as 'peaked' (or 'monoenergetic' if count rate were plotted). 'Peaks' in the spectra occur from ~1 to 4 keV. Energy fluxes as large as 20 ergs cm $^{-2}$ sr $^{-1}$ s $^{-1}$ were observed. If isotropy is assumed, this flux would produce ~100 kR of 5577 Å, enough to saturate the all-sky film, as observed.

Data (courtesy of J. R. Burrows) from several channels of the energetic particle detector (EPD) are presented in Figure 5.

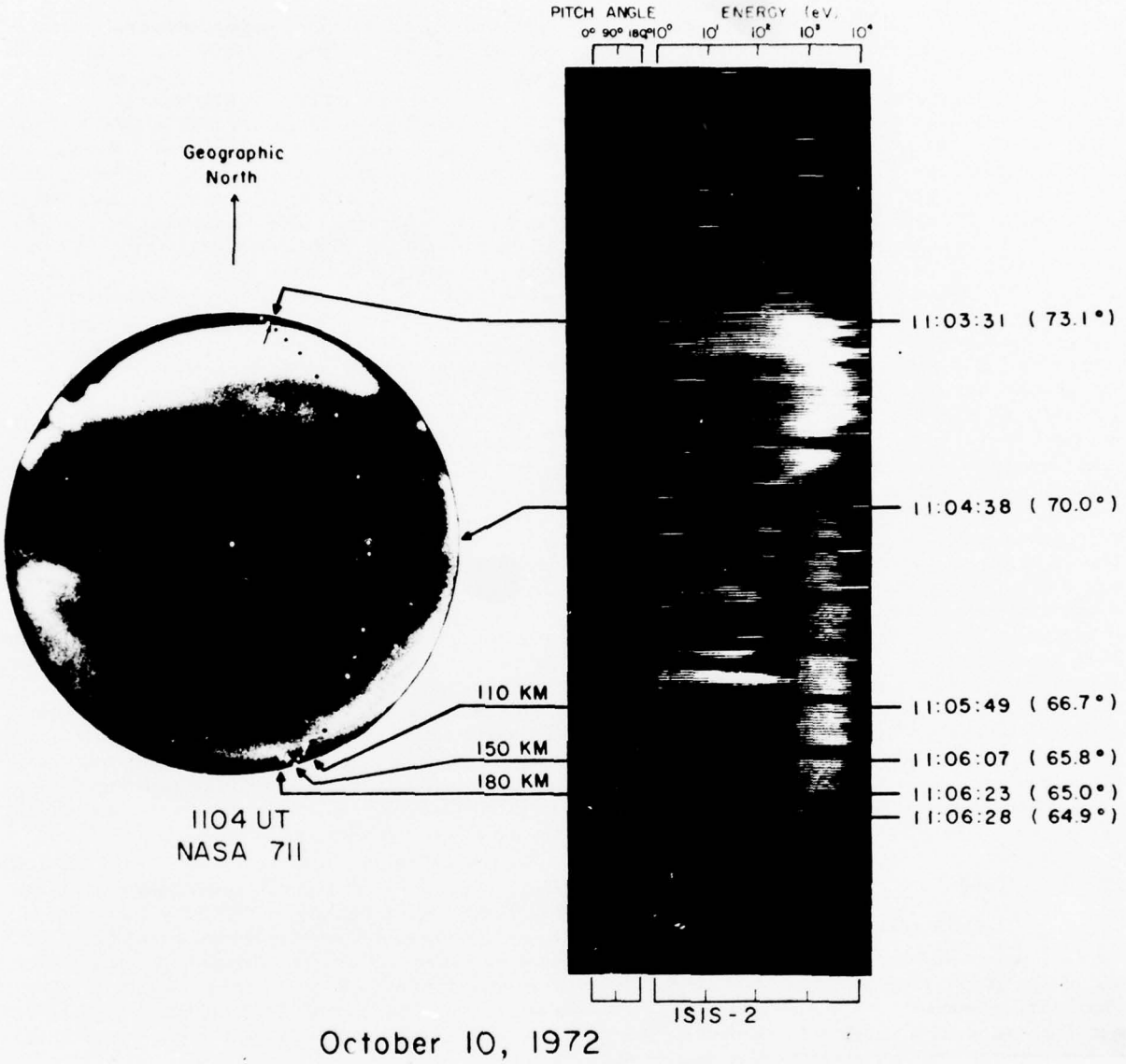

Fig. 3. An all-sky camera photograph corresponding to the closest time of passage of the satellite with the aircraft. The path of the satellite is projected downward along magnetic field lines to the 110-km altitude and shown as dots on the photograph. The times at which the satellite passes various points on the photograph are indicated by arrows, along with the assumed height of the aurora. The southern edge of the particle data corresponds to an auroral altitude of 150–180 km, which is consistent with the characteristic energy of the particles detected at the satellite (see text).

As in the lower-energy data, a change was observed in the EPD fluxes at approximately 1104:30 UT. Equatorward of this point a twice per spin modulated flux with deep minima in both hemispheres was observed. The >200-keV stable trapping boundary was located at this point (Figure 5*f*). Poleward of this boundary the energetic flux softened considerably (see Figures 5*a* and 5*b* for the ratios of the >22- to >40-keV and >40- to 60-keV fluxes) and became structured. It should be noted here that the 'softening' of the high-energy flux is reflected as an increase of the characteristic energy of the electrons measured with the SPS.

All-Sky Camera Observations

The intersection between the poleward edge of the auroral luminosity and the satellite trajectory projected to 110 km is indicated by a black arrow in Figure 3. (Hereafter the satellite location will be the projection to 110 km along the magnetic field.) It can be seen (Figure 3) that except for a very narrow (in latitude) region of soft (average energy less than 1 keV) particle precipitation, the poleward edge of the structured precipitation region coincides with the poleward boundary of the auroral luminosity, in spite of its large zenith angle (about 76°) in the all-sky photograph. The soft particles precipitating just poleward of the discrete aurora might have caused an appreciable luminosity. However, because the average energy is low (see Figure 4*a*), the height of this luminosity must have been higher than 110 km, so that it was likely to be located 'behind' the bright aurora.

If the heights of the equatorward edge of the diffuse aurora are assumed to be 110, 150, and 180 km, the equatorward

boundary of the diffuse aurora on the all-sky photograph can be compared in Figure 3 with that of the diffuse precipitation region on the spectrogram. The point of intersection between the equatorward edge of the auroral luminosity and the satellite path projected down to 110-, 150-, and 180-km heights is shown with the white arrow head, star mark, and triangle, respectively. If the height of the diffuse aurora is assumed to be 110 km, the particle and optical boundaries do not coincide (geographic latitude 66.7° from the all-sky photograph and 64.9° from the spectrogram), and thus the precipitation boundary is located at a lower latitude by approximately 2°. If the height is assumed to be 180 km, they almost coincide with each other (at approximately latitude 65.0°). The energy of electrons must have been near 600 eV to have caused a maximum ionization at 180-km altitude. Indeed, such a value is approximately that of the observed characteristic energy of the particles on the equatorward edge of the precipitation region (see Figure 4*b*).

Another effect which must be accounted for here is that the actual equatorward edge of the diffuse aurora must have been hidden by the lower-altitude part of the diffuse aurora. In fact, the equatorward edge of the diffuse aurora, determined by assuming a 110-km height, corresponds to the point of the highest average energy (approximately 2 keV) in the diffuse precipitation region (at 1105:49 UT; 66.7° geographic latitude, or see Figure 4*f*). As was mentioned earlier, the average energy of the particles gradually decreased equatorward of this point, and therefore the height of the luminosity must have increased (Figure 4*h*). These effects combine to produce the apparent discrepancy between the edges of the precipitation region and luminosity determined from an all-sky camera in the middle of this region.

The diffuse aurora observed by the satellite during this late substorm recovery was the result of the precipitation of Maxwellian electrons, most likely from the inner portion of the plasma sheet (CPS).

PHOTOMETRIC OBSERVATIONS

A 6-in. aperture birefringent filter photometer with a 5° full field of view directed toward the zenith was mounted on the aircraft. This photometer (described by *Deehr* [1969]) is of a type which continuously subtracts the observed background continuum emission signal from narrow discontinuities on the emission continuum. It is therefore most useful for observing the intensity of atomic emission lines, and for the present study these lines were the red and green lines of neutral atomic oxygen at 6300 and 5577 Å, respectively.

The usefulness of these auroral emission lines for determining the characteristic energy of the incoming particle population has been shown by several workers, most recently by *Rees and Luckey* [1974]. Both emissions originate from low, metastable energy levels of neutral atomic oxygen, but the lifetime of the 6300-Å line is considerably longer (110 versus 0.75 s), so this level is collisionally depopulated at a far greater rate at low auroral altitudes. Because both emissions are predominantly excited by secondary electrons whose energy spectrum is, in turn, determined by the characteristics of the incoming primary electrons and because the primary electrons are deposited in altitude inversely according to energy [cf. *Rees*, 1969], the ratio of the intensities of these two lines (6300 Å/5577 Å) is a good measure of the characteristic energy of the incoming primaries.

The intensity of the N_2^+ first negative group is directly related to 5577-Å emission [*Rees and Luckey*, 1974]. The 4278-Å N_2^+ emission may be a better measure of the total ionization than the green line, but it could not be used in the present study because the photometer is not linearly sensitive to emissions of spectral width greater than 6 Å.

Eather and Mende [1972] plotted 6300 Å/4278 Å versus 4278-Å emission as a measure of incoming particle energy for a number of similar aircraft excursions across the auroral zone and found that statistically the lower-energy particles and thus the resulting higher 6300 Å/4278 Å emission ratio were found on the poleward side of the nightside auroral precipitation zone [see also *Mende and Eather*, 1975]. However, this is not always the case, and at times lower characteristic energies could be found at lower latitudes and higher at higher latitudes. For example, the latitudinal distribution of characteristic energy may depend on substorm time [see *Winningham et al.*, 1975].

Figure 6 shows the observed intensity of 6300- and 5577-Å emissions along with the 6300 Å/5577 Å ratio as a function of time throughout the flight. Five areas of different auroral character are indicated in the figure according to Table 1.

The wide variations of the 6300 Å/5577 Å intensity ratio (Figure 6, area 2) are due mostly to viewing the upper and lower borders of moving discrete arcs, which is another indication of the dependence of this ratio on the altitude of the emitting region. The diffuse aurora (Figure 6, area 4), on the other hand, shows a remarkably steady relationship between the two emissions. Plotting the 6300 Å/5577-Å ratio as a function of the 5577-Å intensity (Figure 7) shows, as is generally known, that the brighter the aurora, the more energetic the incoming particles (see next paragraph). Thus all-sky camera pictures can, in general, be a good qualitative indicator of the characteristic energy of the incoming particles; the photometers can, however, provide a quantitative index of the incoming particle energy.

The intensity ratio predicted by *Rees and Luckey* [1974] is shown by solid lines in Figure 7. Because these curves are based on the predicted intensity of 4278-Å N_2^+ ING emission, a conversion to 5577-Å emission was made from Figure 4 of *Rees and Luckey*'s [1974] work. What is shown here is that the characteristic energy α of the incoming electrons varied between approximately 0.2 and 6 keV during the airplane flight. In terms of substorm events this may be summarized in the following way:

1. The initial poleward expanding arc is of low characteristic energy.
2. The bright, discrete poleward arcs immediately following the poleward expansion are associated with electrons of relatively high characteristic energy.
3. The diffuse aurora (after the poleward expansion) has a lower energy characteristic than the bright poleward expanding arc.

Implicit in this result is the support of the Rees and Luckey model for the particle-emission relationship. Indeed, the characteristic energies determined by the photometric data in Figure 7 for each type of aurora match very well the observed particle energy as listed in the last two columns of Table 1. Although the agreement is no better than the assumption that the intensity calibration (comparison with ground-based photometers) is within 50% and that the fluctuations are due to departure from total height integration of the emission.

As mentioned earlier, the particle data from the satellite pass shown in Figure 3 may be regarded as a late substorm snapshot of the latitudinal distribution of auroral precipitation as reconstructed from the photometric data. In other words, at

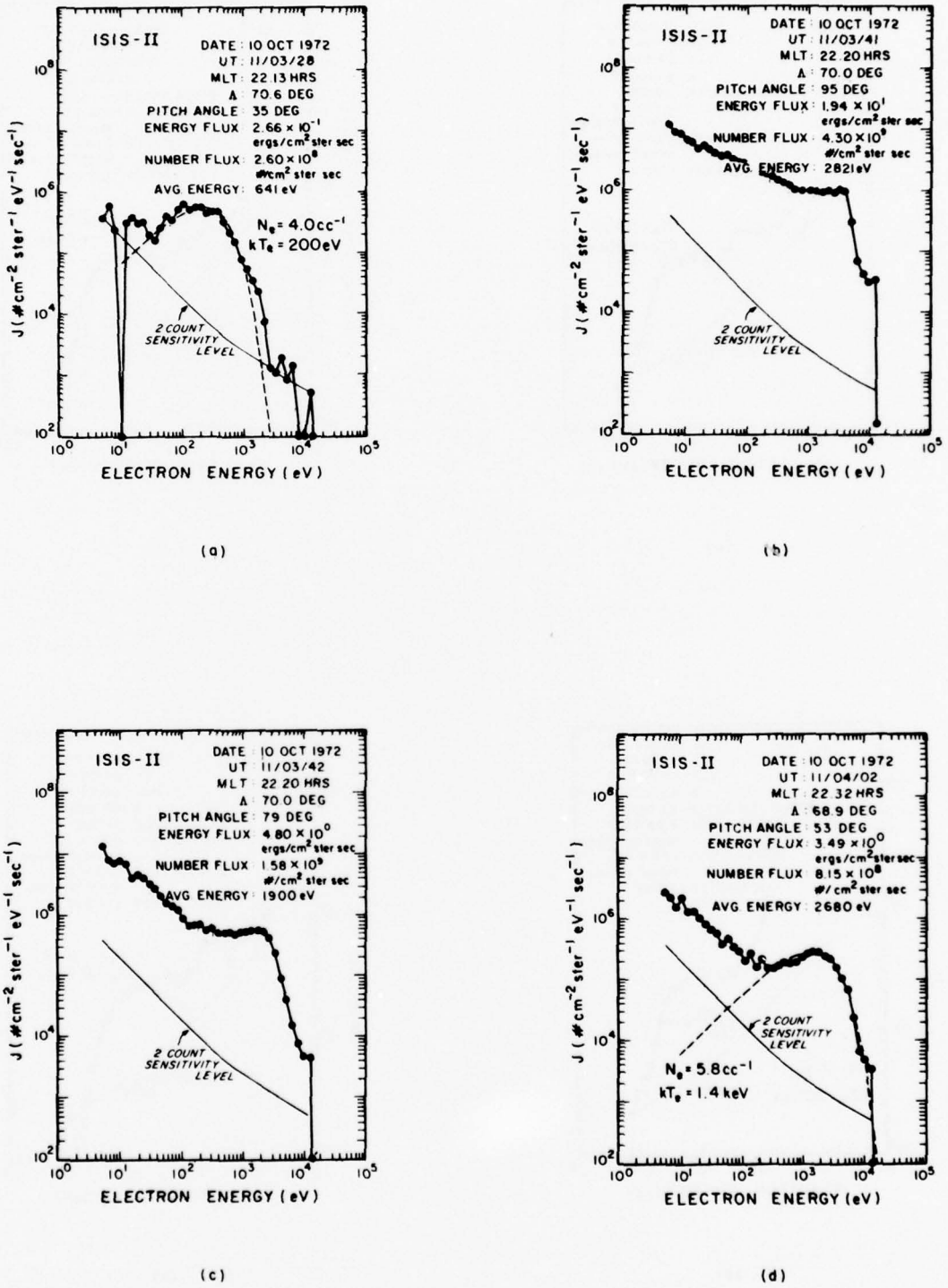

Fig. 4. Eight representative electron differential number flux spectra from the Isis 2 satellite pass 7073. The dots are actual data points, and the dashed lines are least square fits of Maxwellian energy distribution curves which are described by total number flux N_e and characteristic energy $\alpha(kT_e)$.

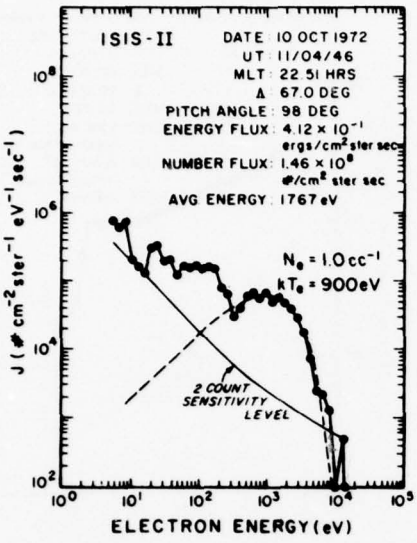

(e)

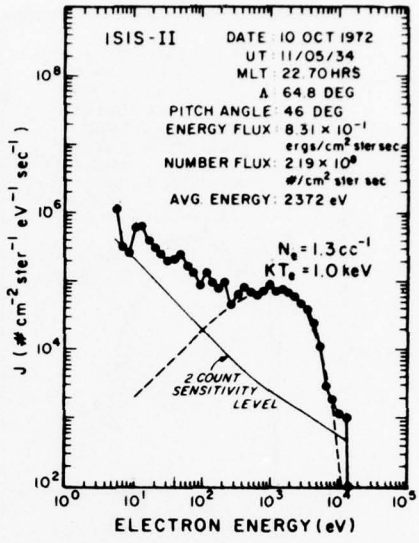

(f)

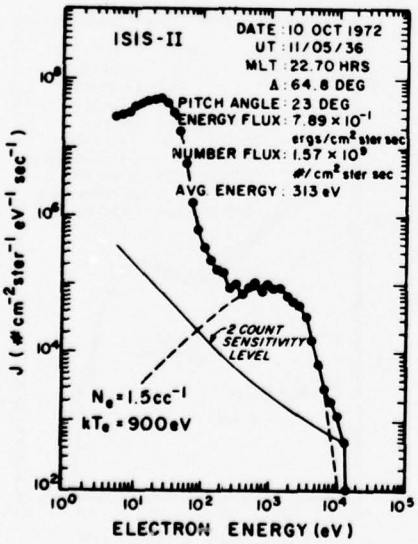

(g)

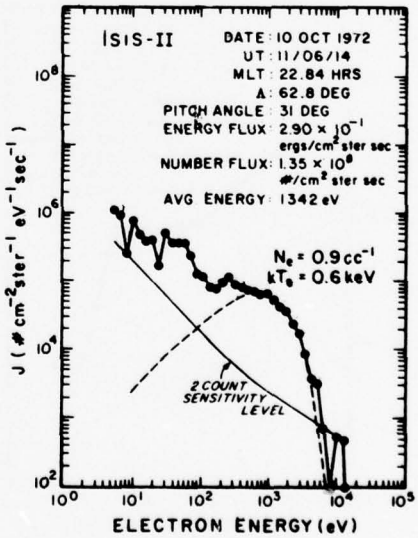

(h)

Fig. 4. (continued)

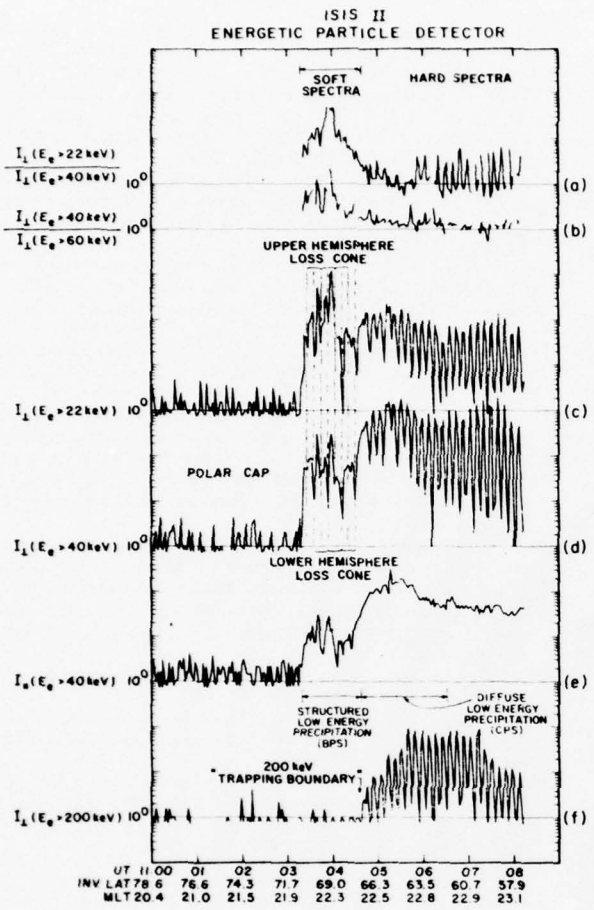

Fig. 5. Energetic particle detector (EPD) data from Isis 2 satellite pass 7073. Parallel and perpendicular markings refer to detector orientation with respect to satellite spin axis (courtesy of J. R. Burrows).

the time of the satellite pass late in the substorm, the latitudinal distribution of characteristic energy determined from the particle data was remarkably similar to that encountered during the course of the substorm from the aircraft according to the photometric observations. Thus the relative latitudinal distribution of particle energy remained roughly the same and appeared to expand accordionlike with the poleward expansion of the substorm. The only region in substorm space-time

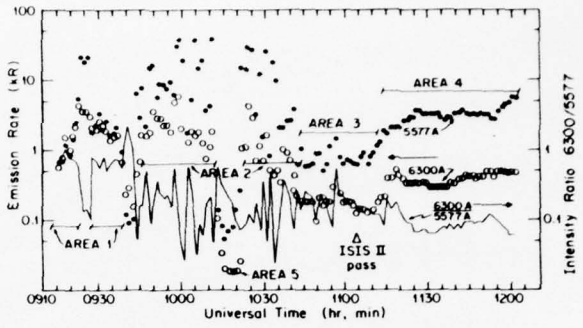

Fig. 6. The zenith intensity of the red (6300 Å) and green (5577 Å) lines of atomic oxygen are shown as open and solid circles, respectively, as a function of universal time during the NASA 990 aircraft flight of October 10, 1972. The intensity ratio is the solid line. The areas covering different auroral features are indicated and explained in Table 1.

not covered by this generalization is the early equatorward (diffuse) aurora (Figure 4*h*), which was equatorward of the airplane throughout the flight.

Another feature of interest is the appearance in Figures 3 and 4*d* of a large flux of low-energy electrons near 1105:36 UT. Although this spectrum indicates an increase of more than a factor of 10 in total number flux, the contribution to the total energy flux is almost nothing. The feature is therefore not visible on the all-sky camera photograph.

Summary

All-sky camera and photometric data were obtained from a jet aircraft as a function of latitude during the course of an auroral substorm. Late in the substorm, near magnetic midnight, the Isis 2 satellite passed near the zenith of the aircraft on a north-south orbit. The position of the discrete and the diffuse auroral regions was determined from the all-sky camera data and compared to the particle data taken by the satellite. Additionally, the ratio of the red (6300 Å) and green (5577 Å) emission lines of atomic oxygen, as a measure of the incoming particle energy, was compared to the particle energy determined from the satellite and to the type of aurora seen on the all-sky camera.

The results of these intercomparisons are as follows:

1. The diffuse and the discrete auroras seen in the all-sky camera data correspond to the two different particle precipitation regions observed from satellites and referred to as CPS and BPS, respectively [*Winningham et al.*, 1975].

TABLE 1. Character of Aurora in the Five Areas Shown in Figure 6

Area	UT, hours	Latitude deg	Type of Aurora	Characteristic Energy	
				Isis 2	Figure 7
1	0915–0923	67	initial poleward expansion arc	200 eV (Fig. 4*a*)	200–600 eV
	0928–0938	68			
2	0923–0928	67.5	bright discrete poleward arcs	>2 keV (non-Maxwellian, see Figs. 4*b*, 4*c*)	<4 keV
	0945–1014	69–73			
	1020–1040	72.5–73			
3	1040–1110	73–69	between diffuse and discrete aurora	900 eV (Fig. 4*e*)	<1.6 keV
4	1115–1200	69–65	diffuse equatorward aurora	1 keV (Fig. 4*f*)	<2 keV
5	0940–0945	69	dark sky poleward of aurora		
	1015–1020	72–72.5			

Figure 2a

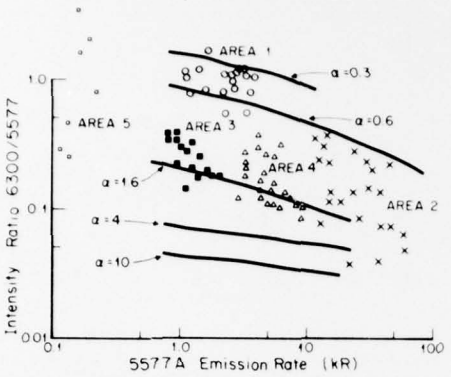

Fig. 7. The 6300 Å/5577 Å intensity ratio as a function of the 5577-Å emission rate. The solid lines indicate the values predicted by *Rees and Luckey* [1974]. The data points are separated according to the areas defined in Figure 6 and Table 1.

2. The diffuse auroral region is associated with stably trapped energetic particles, and the discrete aurora is poleward of the stable trapping boundary.

3. The latitudinal distribution of characteristic particle energies does not change in a relative sense during the poleward expansion but expands accordionlike.

4. The height-integrated intensity ratio of the red (6300 Å) to green (5577 Å) emissions of atomic oxygen is a good indicator of the characteristic energy of the incoming particle spectrum.

Acknowledgments. The UTD portion of this work was supported by NASA grants NGR44-004-150 and NSG 4085 and U.S. Air Force contracts F19628-75-C-0032 and F19628-76-C-0005. The University of Alaska portion was supported by NSF grant ATM74-23832A01 and NASA grant NGR02-001-093.

The Editor thanks I. B. McDiarmid for his assistance in evaluating this paper.

REFERENCES

Deehr, C. S., The twilight enhancement of the auroral and nebular lines of neutral atomic oxygen, *Ann. Geophys., 25*, 881, 1969.

Deehr, C. S., A. Egeland, K. Aarsnes, R. Amundsen, H. R. Lindalen, F. Søraas, P. Stanning, H. Borg, G. Gustafsson, L.-A. Holmgren, W. Riedler, P. A. Smith, G. R. Thomas, and R. Jaeschke, Particle and auroral observations from the Esro 1/Aurorae satellite, *J. Atmos. Terr. Phys., 35*, 1979–2011, 1973.

Eather, R. H., and S. B. Mende, High latitude particle precipitation and source regions in the magnetosphere, in *Magnetosphere-Ionosphere Interactions*, edited by K. Folkestad, Scandinavian University Books, Oslo, Norway, 1972.

Frank, L. A., and K. L. Ackerson, Observations of charged particle precipitation in the auroral zone, *J. Geophys. Res., 76*, 3612, 1971.

Hoffman, R. A., and J. L. Burch, Electron precipitation patterns and substorm morphology, *J. Geophys. Res., 78*, 2867, 1973.

Lui, A. T. Y., and C. D. Anger, A uniform belt of diffuse auroral emission seen by the Isis-2 scanning photometer, *Planet. Space Sci., 21*, 799, 1973.

Lui, A. T. Y., C. D. Anger, D. Venkatesan, W. Sawchuck, and S.-I. Akasofu, The topology of the auroral oval as seen by the Isis 2 scanning auroral photometer, *J. Geophys. Res., 80*, 1795, 1975.

Mende, S. B., and R. H. Eather, Spectroscopic determination of the characteristics of precipitating auroral particles, *J. Geophys. Res., 80*, 3211, 1975.

Rees, M. H., Effects of low energy electron precipitation on the upper atmosphere, in *The Polar Ionosphere and Magnetospheric Processes*, edited by G. Skovli, Gordon and Breach, New York, 1969.

Rees, M. H., and D. Luckey, Auroral electron energy derived from ratio of spectroscopic emissions, 1, Model computations, *J. Geophys. Res., 79*, 5181, 1974.

Sharber, J. R., and W. J. Heikkila, Fermi acceleration of auroral particles, *J. Geophys. Res., 77*, 3397, 1972.

Snyder, A. L., S.-I. Akasofu, and T. N. Davis, Auroral substorms observed from above the north polar region by a satellite, *J. Geophys. Res., 79*, 1393, 1974.

Winningham, J. D., F. Yasuhara, S.-I. Akasofu, and W. J. Heikkila, The latitudinal morphology of 10-eV to 10-keV electron fluxes during magnetically quiet and disturbed times in the 2100–0300 MLT sector, *J. Geophys. Res., 72*, 3148, 1975.

(Received February 18, 1976;
accepted July 28, 1976.)

Figure 2b

VOL. 81, NO. 34 JOURNAL OF GEOPHYSICAL RESEARCH DECEMBER 1, 1976

The Topside Magnetospheric Cleft Ionosphere Observed From the Isis 2 Spacecraft

G. G. SHEPHERD,[1] J. H. WHITTEKER,[2] J. D. WINNINGHAM,[3] J. H. HOFFMAN,[3] E. J. MAIER,[4] L. H. BRACE,[4] J. R. BURROWS,[5] AND L. L. COGGER[6]

Data from the Isis 2 spacecraft for five orbits in November 1971 are examined in detail. The spacecraft was then in cartwheel configuration, permitting detailed angular and spectral measurements of charged particle fluxes ($E > 5$ eV), local ion densities and temperatures, local electron densities and temperatures, F region peak electron densities, and 6300- and 5577-Å emissions accurately located at the field line foot. In the November 9 and 10 orbits, highly structured regions of electron flux having average energies of ~0.7 and ~0.2 keV are observed. The O^+ density at the 1400-km spacecraft altitude generally reflects the electron precipitation, disappearing rapidly at the poleward boundary with He^+ becoming dominant in the polar cap. Throughout this region of enhanced O^+ densities, strong polar wind flows of H^+ are observed. The electron densities obtained with the topside sounder are sometimes higher than the ion densities; this is in part due to the structured nature of the cleft region, but other indirect plasma processes may also be involved. The ion temperature is about 2000°K inside the cleft and rises to about 5000°K at the poleward cleft boundary. The F region peak density shows some structure but no uniquely identifiable cleft response, and the optical emissions generally show a multiple peaked structure, normally with the lowest red/green ratio in the equatorward components. The November 17 and 18 orbits differ in that the electron spectrum precipitation energies are closer to 100 eV, are less structured, and are displaced to higher invariant latitude. The O^+ densities are higher, while the light ions are little changed, and O^+ is observed poleward of the precipitation region, implying strong convection perpendicular to the auroral oval. The optical red/green ratio is higher for these orbits. A tentative explanation for the different behavior is the passage of a sector boundary between these two dates with the interplanetary field direction changing from 'away' to 'toward.'

INTRODUCTION

The existence of dayside aurora and the continuity of the auroral oval have been known for some time [*Feldstein*, 1963]. Studies of the polar cap ionosphere had revealed topside density enhancements attributable to particle energy input on the earth's dayside [*Nishida*, 1967; *Sato and Colin*, 1969]. But the recognition of the magnetospheric dayside cusps [*Heikkila and Winningham*, 1971; *Frank and Ackerson*, 1971] or cleft [*Heikkila*, 1972] came about through the observation of magnetosheathlike plasma at low altitudes and high latitudes on the earth's dayside. Subsequently, many manifestations of this dayside energy source have been identified and studied [*Vasyliunas*, 1974]. Pronounced ionospheric characteristics are elevated electron temperature [*Brace and Miller*, 1974] and F region irregularities [*Dyson and Winningham*, 1974; *Ahmed and Sagalyn*, 1973]. *Whalen and Pike* [1973] related the F region irregularity zone to the occurrence of 6300-Å emission, a direct indicator of incident low-energy electrons.

The role of the cleft as an ionization source for the polar cap is a topic of current study; *Knudsen* [1974] discussed the plausibility of this in terms of the convection pattern in the polar cap. But a more recent study [*Knudsen et al.*, 1975] suggests that the ionospheric residence time in the cleft is too short to provide a significant effect. *Whitteker* [1976] has given a detailed review and thorough discussion of ionospheric cleft effects.

The Isis 2 spacecraft offers an opportunity to measure the cleft particle fluxes and ionospheric response at 1400 km as well as topside electron density profiles and F region peak densities. The optical emissions at 6300, 5577, and 3914 Å can also be detected with the on-board photometers. This paper reports upon a detailed and coordinated set of observations for a few orbits in November 1971. This period was chosen because the orbit then had a suitable local time, the spacecraft was in cartwheel configuration for good measurements of local parameters, and the polar cap was reasonably dark for optical viewing.

DATA ACQUISITION

A brief description of the instruments and a list of relevant references has been given by *Shepherd et al.* [1973]. For this study a period of cartwheel configuration was chosen (spin axis perpendicular to the orbit plane) in order to obtain the best ion data. In this mode a complete scan about the velocity vector is obtained once every spin (roughly 18 s). In addition, a complete pitch angle scan is obtained with the particle detectors.

As will be seen in the data, there is considerable fine structure present in the local plasma. For this reason, caution should be exercised in comparing the results from experiments which nominally measure the same parameter. For example, both the ion mass spectrometer (IMS) and the retarding potential analyzer (RPA) measure ion density, but since the sensors are located about 90° apart on the spacecraft, the 'simultaneous' samples analyzed are separated by about 5 s in time and 35 km in space. For one instrument the data points are separated by about 125 km. Thus what sometimes appears to be a discrepancy in the density profile observations along the spacecraft track is simply a measure of the fine-scale structure of the ambient medium. This is to be contrasted with the local density determinations provided by the sounder, which, it is estimated, represent a measurement over a scale size of

[1] Centre for Research in Experimental Space Science, York University, Toronto, Ontario, Canada.
[2] Communications Research Centre, Ottawa, Ontario, Canada.
[3] Center for Space Sciences, University of Texas at Dallas, Richardson, Texas 75082.
[4] Goddard Space Flight Center, Greenbelt, Maryland 20771.
[5] Herzberg Astrophysical Institute, National Research Council, Ottawa, Ontario Canada.
[6] Physics Department, University of Calgary, Calgary, Alberta, Canada.

Figure 2c

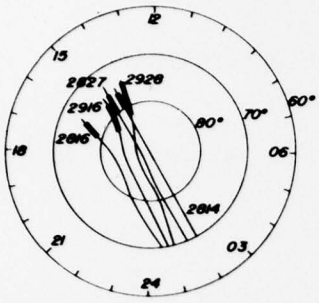

Fig. 1. Invariant polar projection, showing the spacecraft tracks labeled by orbit number, for the orbits used in this study. The regions of cleft precipitation are shown by the thickened traces.

about 1 km and which are obtained alternately at intervals of 100 and 300 km. A further complication is that the existence of sufficiently rapid local variation (which often occurs) precludes the reduction of the RPA current-voltage curves to determine the ambient ion temperature. This lack of continuous (once per spacecraft rotation) ion temperature data should be considered in interpreting temperature differences in the various regions.

The two-dimensional mapping capability for the optical data is not available, since the scanning occurs repeatedly along the spacecraft track. The consequent high redundancy of the data is used here to minimize the delay time between the acquisition of the optical data and the direct measurements made at the spacecraft on the field line connected to the emitting region. This is achieved simply by selecting optical data from the single spin giving the minimum time delay for the center of the cleft region. It was also possible to inspect adjacent spins to confirm that temporal variations were not significant. The individual optical data points are obtained at 45 Hz for the auroral scanning photometer (ASP) and 30 Hz for the red line photometer (RLP), and though they are converted to equivalent spacecraft time for the plots shown, each is obtained in roughly 1 s of viewing time, so that it is an instantaneous pattern that is presented.

DATA PRESENTATION

Figure 1 is a polar plot in invariant coordinates, showing the paths of the Isis 2 spacecraft for the passes used in this study. The extent of the cleft precipitation for each orbit is shown by the thickened portion along each path. The magnetic times for the cleft crossings vary within a range of a few hours following local magnetic noon.

Orbit 2816

Figure 2 shows a composite of the results obtained from orbit 2816 on November 9, 1971, at 0947 UT. The top frame shows the soft particle spectrometer (SPS) electron data in the format described by *Heikkila and Winningham* [1971]. The magnetic local time and invariant latitude are shown along the top of this frame, and the invariant latitude is hand lettered below for clarity. The second frame is from the 150-eV electron channel of the energetic particle detector (EPD) experiment. It will be seen later that the cleft electron energies are sometimes sufficiently low to be entirely below the threshold of this detector; comparison of this channel with the SPS data thus gives a very sensitive indication of energy spectral changes. In this particular orbit the EPD channel has four flux peaks. The most equatorward one near 76.3° invariant is the broadest and is at the poleward limit of a keV flux continuum that starts at 74.6°. The SPS shows its maximum energy flux centered at 0.7 keV in this feature. The three more poleward peaks extending to 78° are narrower and more discrete, and the SPS shows that their average energy softens toward 0.2 keV with increasing latitude. The keV flux may be characteristic of 16.5 hours magnetic local time, which is rather far into the afternoon to be classified as a cleft pass. No protons were observed, which is also characteristic of the late afternoon sector. The other orbits to be shown will be presented in order of increasing proximity to local magnetic noon.

The next frame, labeled SDR (sounder), shows the local electron density obtained at 1400 km by the topside sounder; it is sharply peaked in its latitude distribution, not at the center of the cleft precipitation but at its poleward edge, 1° of latitude away. The density enhancement in the vicinity of the cleft is about a factor of 3. The next lower frame, labeled IMS, contains the ion mass spectrometer local ion densities, showing a marked O^+ response over the entire region of energetic electron energy input. Since the IMS has been intercalibrated against the SDR, the differences between the two are unexpected. Closer examination of individual data points shows that the single high point in the SDR local density was taken close to an EPD (and SPS) flux peak, while the closest IMS point was in the trough between two electron flux peaks. This point will be discussed later. The O^+ density drops sharply at the poleward cleft boundary, beyond which He^+ becomes the dominant ion, with several times the density of H^+. Throughout this region (the polar cap) the O^+ is virtually absent, and below the threshold of the IMS, a few ions per cubic centimeter. The thickened base line of this frame indicates the region where polar wind flows of H^+ ions are observed by the IMS to be greater than 1 km/s. The flow is seen to occur throughout the O^+ enhancement region. The next lower frame (SDR) shows the electron densities measured at the *F* region peak and indicates variations of the order of 50% in the region of the cleft energy source.

The bottom frame contains the optical emission rates for the 6300- and 5577-Å lines, obtained from a single spin as described earlier. Multiple peaks are evident, superimposed on a background that rises in the equatorward direction in response to local twilight. The most equatorward peak is strongest, at 76.3° invariant. In it the 5577-Å intensity exceeds that at 6300 Å, and this corresponds well to the equatorward flux peak with average energy near 0.7 keV. The adjacent poleward peak has roughly equal 5577-Å and 6300-Å intensities and seems to correspond to the narrow pair of electron flux peaks at 77.0° invariant, which are unresolved in this viewing geometry. A weak peak, still further poleward at 77.8° invariant, corresponds to the very narrow 0.2-keV flux seen there. These multiple features appear to be auroral arcs, which are characteristic of the late afternoon sector [*Shepherd et al.*, 1976].

Orbit 2827

This pass occurred November 10, 1971, at 0638 UT and a local magnetic time of 14.5 hours; the composite data are shown in Figure 3. As in orbit 2816, there is a lower-latitude keV flux continuum from 75.0° to 78.2° invariant, while the discrete features extend as far as 79.6°. (Note the SPS data absence due to command sequencing near 77.4°.) The more poleward region of precipitation is characterized by narrow discrete fluxes having average energies of $\lesssim$0.2 keV, the two most poleward features having energies below the EPD thresh-

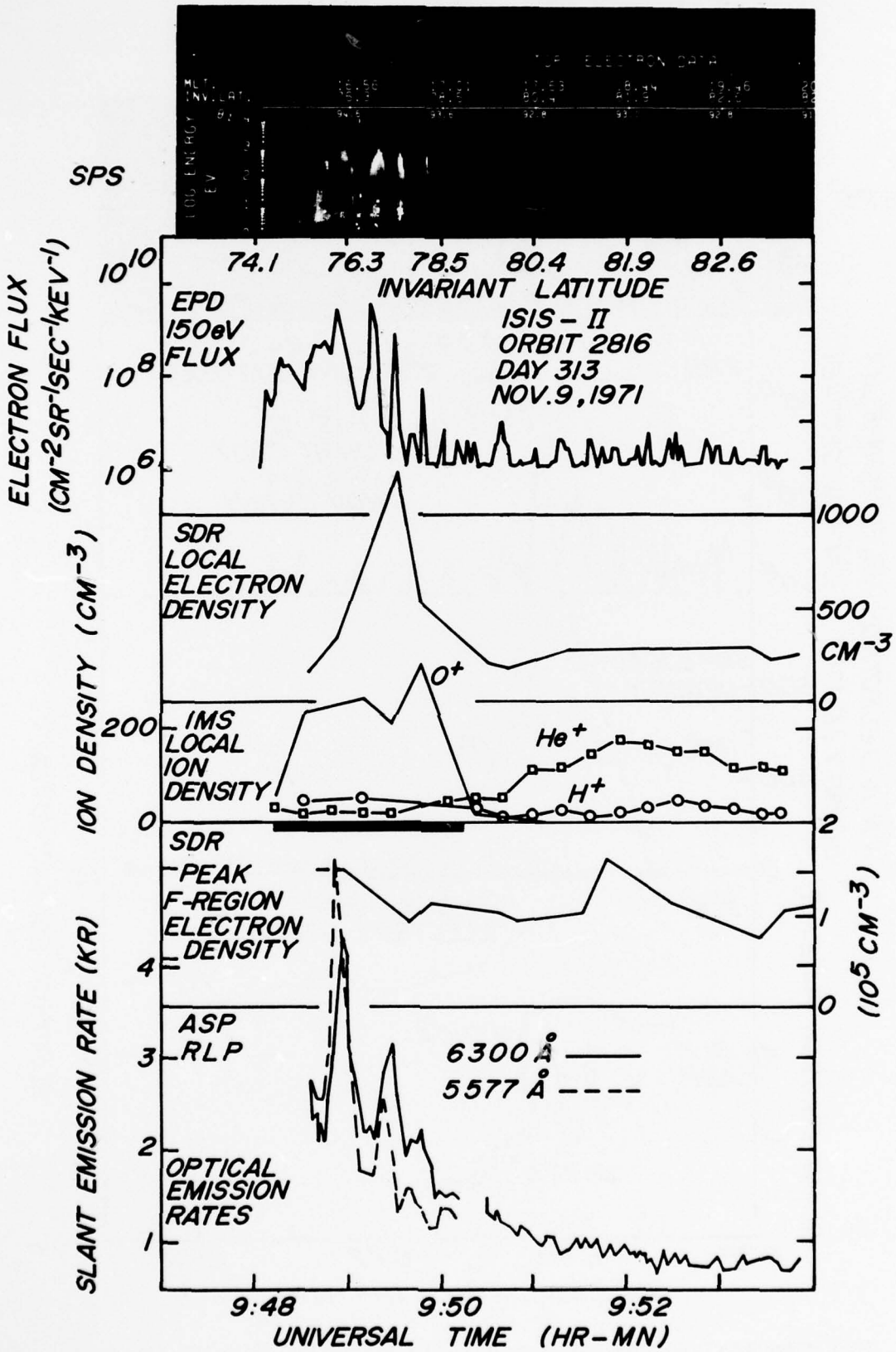

Fig. 2. Collected Isis 2 data for orbit 2816, November 9, 1971, at 16.5 hours MLT. The universal time shown at the bottom is the time at which the spacecraft crossed the field line to which all data relate, and the spacecraft invariant latitude is shown at the top. The top frame is an SPS electron spectrogram where the vertical direction is energy and the trace density indicates flux. The vertical bars extending over the whole energy range are sun pulses in the instrument. Successive frames downward show data from the EPD 150-eV channel, SDR local electron density, IMS, ion composition and regions of H^+ flow being indicated by the thick base line, SDR-measured F region peak density, RLP 6300-Å measurements, and ASP 5577-Å data.

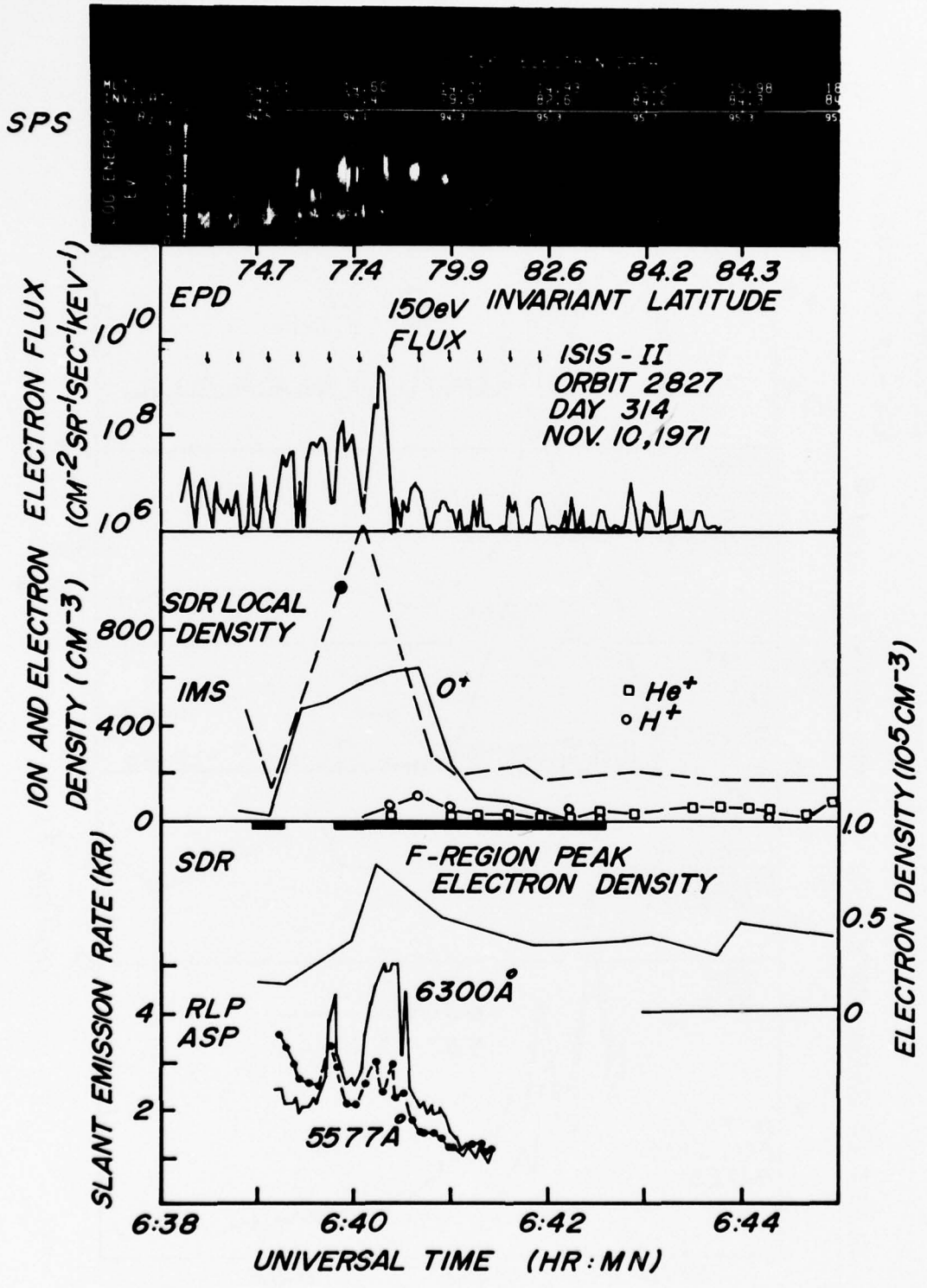

Fig. 3. Collected Isis 2 data for orbit 2827, November 10, 1971, at 14.5 hours MLT. The sequence of short arrows indicates the times at which the EPD and SPS were looking down the field line. The caption of Figure 2 applies to this figure also.

old. Both the SPS and the EPD fluxes show periodic minima at about 18-s intervals due to scanning through the atmospheric loss cone; the times of downward viewing are shown by the series of short vertical arrows in the figure. The small EPD flux peaks poleward of 78.2° invariant arise from sunlight, and these 'sun pulses' are manifested in the SPS spectrogram as weak vertical bars. A weak proton flux (not shown) ended at 0640:45, at about the same time as the termination of the electron flux.

Again in this pass the SDR local density has an isolated peak density about twice that shown by the IMS for which the O^+ density is again relatively uniform across the precipitation region. The solid circle (the only point not visible as a discontinuity in slope in the straight line connection of discrete points used here) on the dashed curve just prior to the SDR peak is a second consistent high-density point, suggesting that the explanation offered before of a chance high flux coincidence may be inadequate. In a stream of 5×10^{10} electrons cm^{-2} s^{-1} of 100-eV energy the number density is about 10^6 el cm^{-3}. This is only 1 order of magnitude below the ambient densities, and the ionospheric response to this charge input may involve electric fields and waves that affect the electron and ion measurements differently. In addition, the SDR samples a 1-km region around the spacecraft and is therefore much more likely than the IMS to be within sampling range of one of the discrete flux regions.

As in the previous example, the O^+ drops sharply at the poleward boundary, with a slight tail extending to 83.0° invariant in this case, beyond which He^+ becomes the dominant ion. The H^+ flow shows a slight break near its equatorward edge. The *F* region peak density has a significant response to the largest EPD peak, which also coincides with the peaking of a broad optical emission having a red/green ratio of about 4. There is a narrow equatorward flux peak with a red/green ratio of 2.5 that coincides with the 0.7-keV flux peak at 77.1° invariant. The 6300-A emission is the stronger of the two at all latitudes, and this reddening may be attributed to closer proximity to magnetic noon.

Orbit 2814

The data from this orbit, shown in Figure 4, were taken two orbits prior to that of Figure 2, November 9, 1971, at 0600 UT with a magnetic local time of 14.1 hours. There is a keV flux continuum present from 76.0° to 79.0° invariant, with intense flux bursts at 79.4°, 78.9°, and 79.6° invariant extending in energy from 0.1 to 1 keV. Equatorward of these bursts there are several others centered near 0.1 keV and one very narrow intense flux at 77.6° having energies from 5 to 100 eV, evident only in the SPS spectrogram. A weak proton flux ended at 0603:00 UT. Both the SDR density and the IMS O^+ density show a double-peaked response to these distinct regions of $\simeq$1-keV precipitation (there is an SPS data absence near the equatorward peak), and the absolute density values agree as well. This shows that the differences between the electron and ion densities seen in other orbits do not arise from a consistent error such as in calibration. It is also appropriate to note here that these apparent differences between electron and ion densities do not occur at lower latitudes; they are a polar cap phenomenon.

For this orbit, RPA densities and temperatures were also available and are shown. Apart from the region near 79.0° these densities generally agree with the SDR densities, but the temperature results are surprising at first sight, showing values below 2000°K in the region of energy input and nearly 5000°K in a narrow region just at the poleward cleft boundary. But a numerical model of topside dynamics (J. H. Whitteker, unpublished manuscript, 1976) accounts for this behavior as adiabatic heating of the ions when the poleward convecting topside ionosphere collapses as a result of the drop in electron temperature when the convecting plasma leaves the region of precipitation. Further in the polar cap, high values of about 3500°K are observed. The RPA also indicated the presence of wavelike plasma structures from 0601:20 to 0603:11 UT (the region of precipitation) and again at 0606:35 (in the polar cap region of high ion temperature). In the IMS data, He^+ again becomes dominant poleward of the cleft, although O^+ reappears in the ion temperature enhancement at 0606. Again, the H^+ flows follow the O^+ enhancement region.

The *F* region peak densities show a curious weak depression in the cleft region. There are again two well-defined optical peaks, the equatorward one being more intense, at 2.5 kR of 6300-Å emission. Unlike the two preceding orbits, it has the higher optical red/green ratio and appears to correspond to the very narrow intense SPS feature at 77.6° mentioned earlier, which occurred when the SPS was sampling pitch angles, θ_p, in the downcoming (precipitating) loss cone. The poleward feature appears to correspond to the unresolved features at 78.2° and 78.7°.

Orbit 2928

These data, obtained November 18, 1971, at 0600 UT and shown in Figure 5, are dramatically different from the preceding examples. They are taken closer to magnetic noon, at 13.8 hours, which may be a partial explanation. The flux measured by the SPS is less structured and spreads over a broader region, while the absence of any significant EPD response shows that the energies involved are much lower. The weak proton flux terminates at 0602:30, at the same location as the electrons. There is a rising base line level in the 5-eV threshold level that makes the electron energy appear higher than it actually is in the poleward region. The SDR local density peaks at the poleward boundary, with much larger densities present, about 4000 cm^{-3} compared to typically 800 cm^{-3} in the previous examples. The precipitating energy flux does not have instantaneous values exceeding those of previous orbits, about 1 erg cm^{-2} sr^{-1} s^{-1}. The O^+ response is similar to the SDR response, rising gradually through the cleft region and dropping abruptly at the poleward boundary, well beyond the region of maximum energy input. The He^+ and H^+ densities (multiplied by 10 on the plot) are not much affected by this substantial increase in O^+, except that H^+ now exceeds He^+, and the light ions are not dominant in the polar cap. The H^+ flows are found throughout the region with the maximum velocities at the poleward side, where the O^+ concentration is lowest. The *F* region densities may be affected by the energy input, though one cannot be certain. The optical responses are dramatic, with a feeble 5577-Å response in contrast with a 6300-Å emission rate of about 4 kR above background. One can still imagine a double-peaked structure with no green component at all in the poleward peak and only a weak one in the equatorward features. The region of bright 6300-Å emission has sharply defined boundaries, at 74.7° and 79.0° invariant, with an extension into the polar cap not seen on earlier passes. The red/green ratio measured above background appears to be about 8. All of this is consistent with a dramatic softening of the total energy input, producing a large increase in 6300-Å emission and much enhanced O^+ densities at the spacecraft.

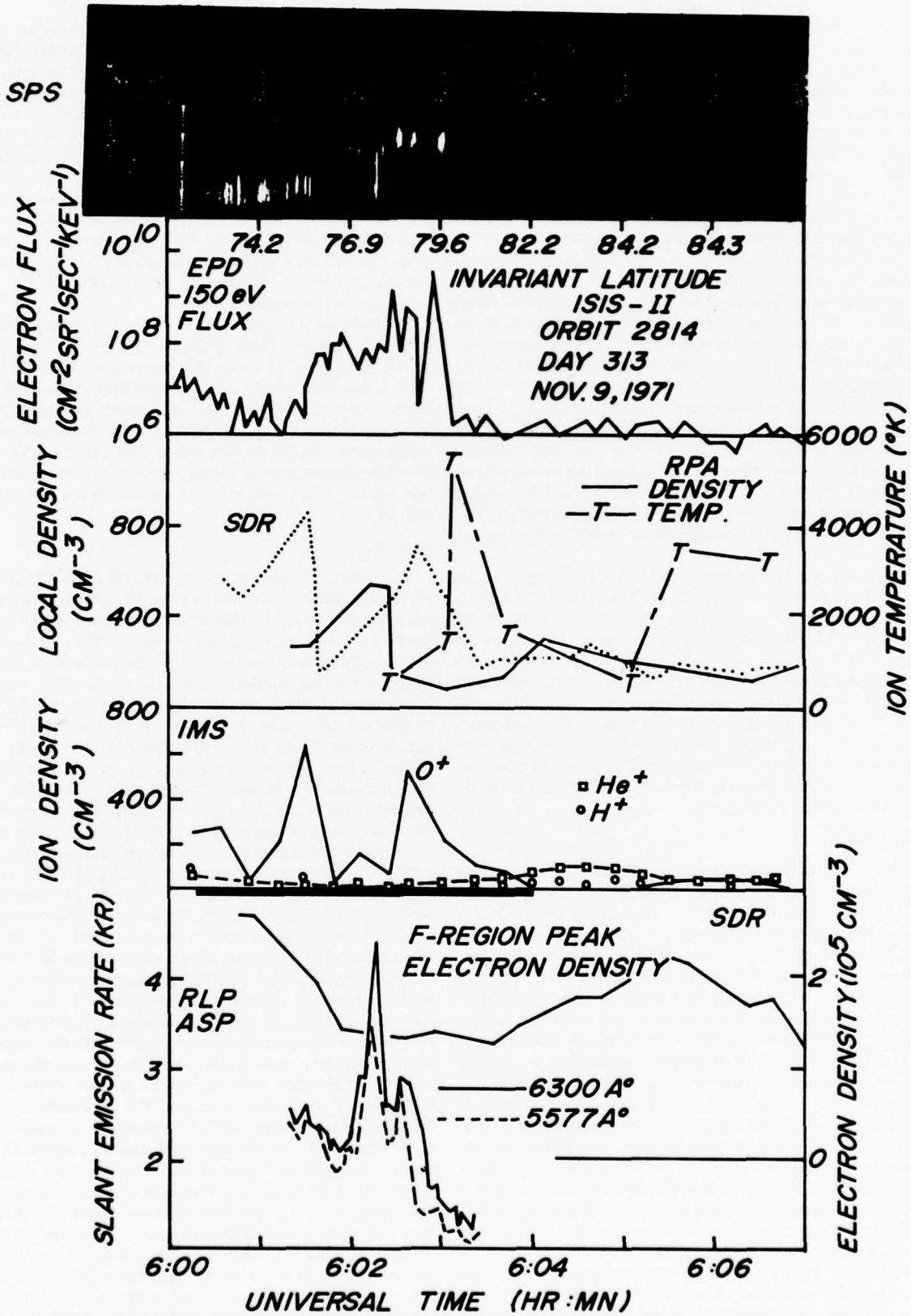

Fig. 4. Collected Isis 2 data for orbit 2814, November 9, 1971, at 14.1 hours MLT. The caption of Figure 2 applies, except that a frame of RPA data is added. The symbol *T* connected by a broken line indicates ion temperature; the solid curve indicates RPA total ion density, which is compared with the SDR local electron density.

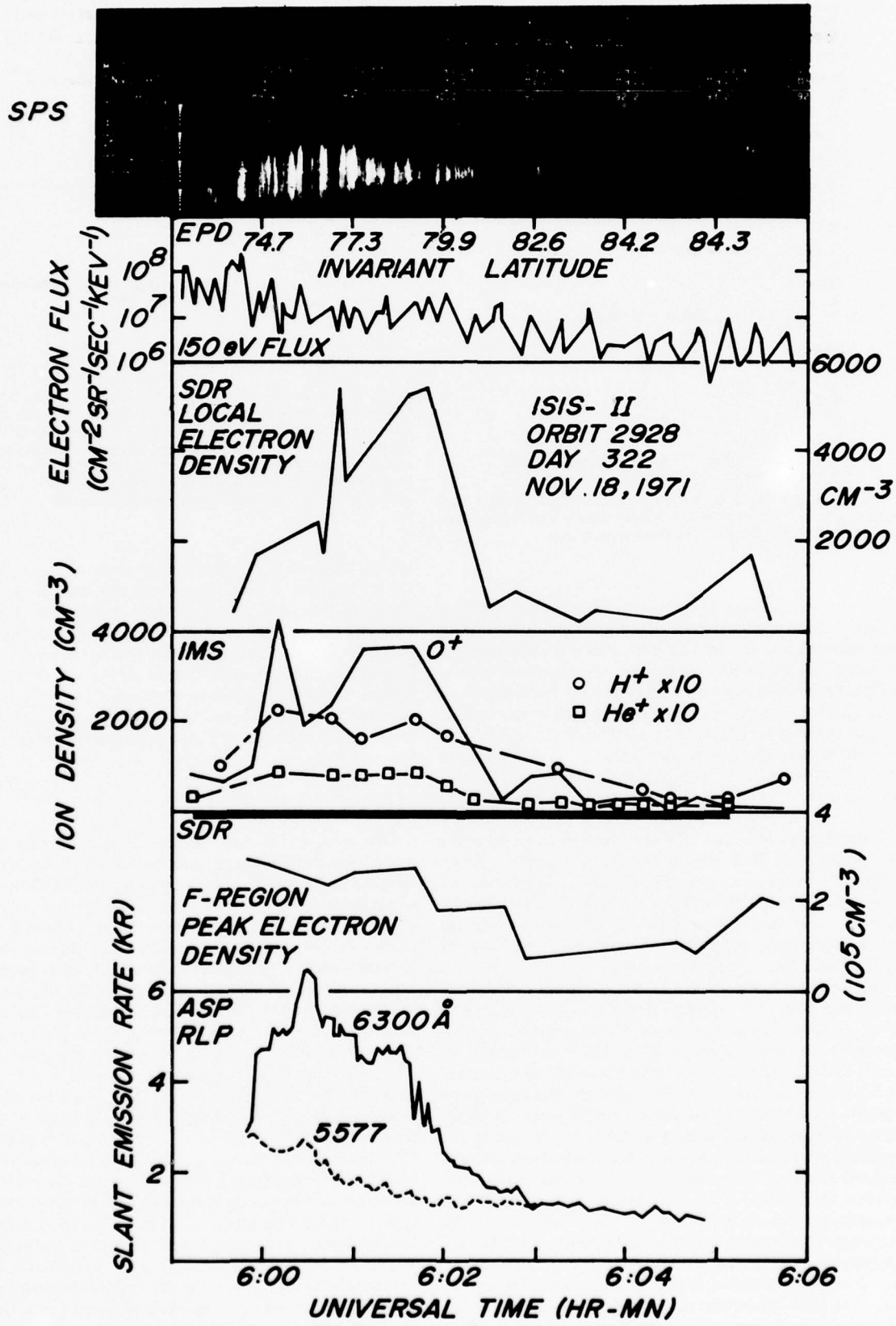

Fig. 5. Collected Isis 2 data for orbit 2928, November 18, 1971, at 13.8 hours MLT. The caption of Figure 2 applies; further data for this orbit are shown in Figure 6.

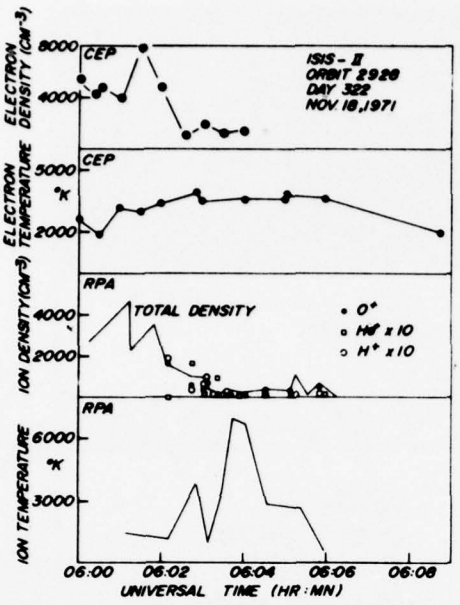

Fig. 6. Further Isis 2 data from orbit 2928 (see Figure 5 also) containing CEP measurements of electron density and temperature, compared with RPA ion densities and temperatures.

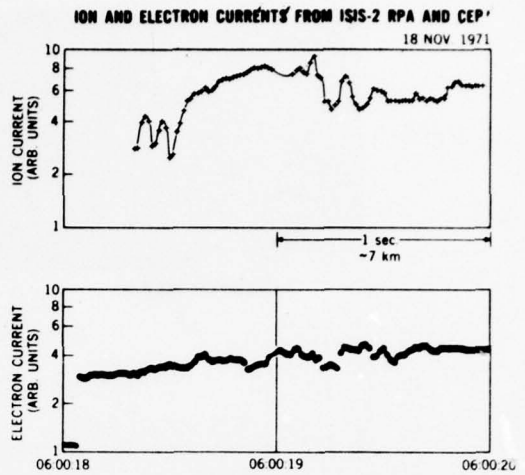

Fig. 7. Ion and electron currents measured by the Isis 2 RPA and CEP for 2 s at 0600:18 UT on November 18, 1971, showing the small-scale structure present in the plasma. The current to the CEP (primarily electrons) is measured with the sweep voltage held constant at +4 V with respect to the spacecraft. Current to the RPA (primarily ions) is measured with the retarding voltage sweeping at a rate very slow compared to the scale times of the structure detected.

The electron densities at the spacecraft are sufficiently high to permit electron temperature values to be obtained with the cylindrical electrostatic probe (CEP). This was not possible in the orbits previously shown because the spacecraft was in sunlight (producing photoelectrons) and the ionosphere was dark, yielding low densities. The results are shown in Figure 6, along with those obtained from the RPA. Both the RPA and the CEP show a sharp response in plasma density about at 0601 UT, at the center of the region of energy input. The RPA densities are in accord with those obtained from the SDR and the IMS, and apart from one high point at 0601:40, with the CEP densities as well. The SDR electron density peaks at the same location as does the CEP-measured electron density, though at a lower absolute value. The electron temperature shows little variation poleward of the cleft, at about 3500°K, while the ion temperature shows a pronounced rise, to 7000°K, poleward of the cleft, as seen before in orbit 2814 and explained as adiabatic collapse heating.

Fine structure in the plasma density is present sporadically during this pass. An example of the wavelike structure is shown in Figure 7, which shows 2 s of data obtained simultaneously by the CEP and by the RPA. The lower curve is the current to the cylindrical probe when it was held at a constant +4-V potential with respect to the spacecraft. The upper curve is the ion current observation from the RPA when the sweep voltage change was not causing a significant change in the magnitude of the current. Some of the fine-scale structure is present in the same phase relationship in the two signals. This implies a modulation of the local plasma density (both ions and electrons) in both space and time. Note that some of the fine structure in the electron data has extremely sharp boundaries, appearing as discontinuities in the current, whereas the corresponding boundaries in the ion data are often not so sharp. The RPA instrument time response is adequate to follow the current changes as shown in the electron data. Thus the differences are real and presumably arise from the ionospheric response to the precipitating electrons, as conjectured for the apparent differences in SDR and IMS densities. The fractional changes in density for the two species are noticeably different, the fluctuations in the ion current being larger than the corresponding fluctuation in the electron current. This may be a further indication that the ion plasma was the driven, or excited, component receiving its stimulus from the energetic electrons present in the region. A more complete survey of the small-scale structures in the cleft region will be the subject of a separate study.

Orbit 2916

This orbit, at 15.0 hours magnetic time, is shown here because it has characteristics similar to those of orbit 2928, even though its magnetic time is similar to the times of the first three orbits presented. It was acquired on November 17, 1971, at 0717 UT, and the data are shown in Figure 8. The SPS shows a fairly compact region with energies below 300 eV and with little prominent structure. There is a weak EPD response to ~79° invariant and only sun pulses thereafter. The weak proton flux ends at 0718:20 UT somewhat before the electron flux disappears. The SDR local density again is peaked near the poleward boundary and trails off far into the polar cap, to 83.3° invariant. The O^+ peak from the IMS is also sharply peaked with a density of about half that of the sounder. In a fashion not inconsistent with the SDR densities the O^+ density shows a smaller but significant (300 ions cm^{-3}) level up to 83.3° invariant as well, substantially poleward of the poleward boundary of precipitation. The characteristic rise of He^+ does not occur until this point is reached. The H^+ flows are found again throughout the region of O^+ enhancement. The *F* region density shows a pronounced cleft response in the same location as the local electron density peak. The 6300-Å optical emission shows four distinct regions that can be identified with SPS flux regions, the equatorward component at 2.5 kR being the most intense. The spike of 5577-Å emission cannot be associated with a flux feature and appears to be transient.

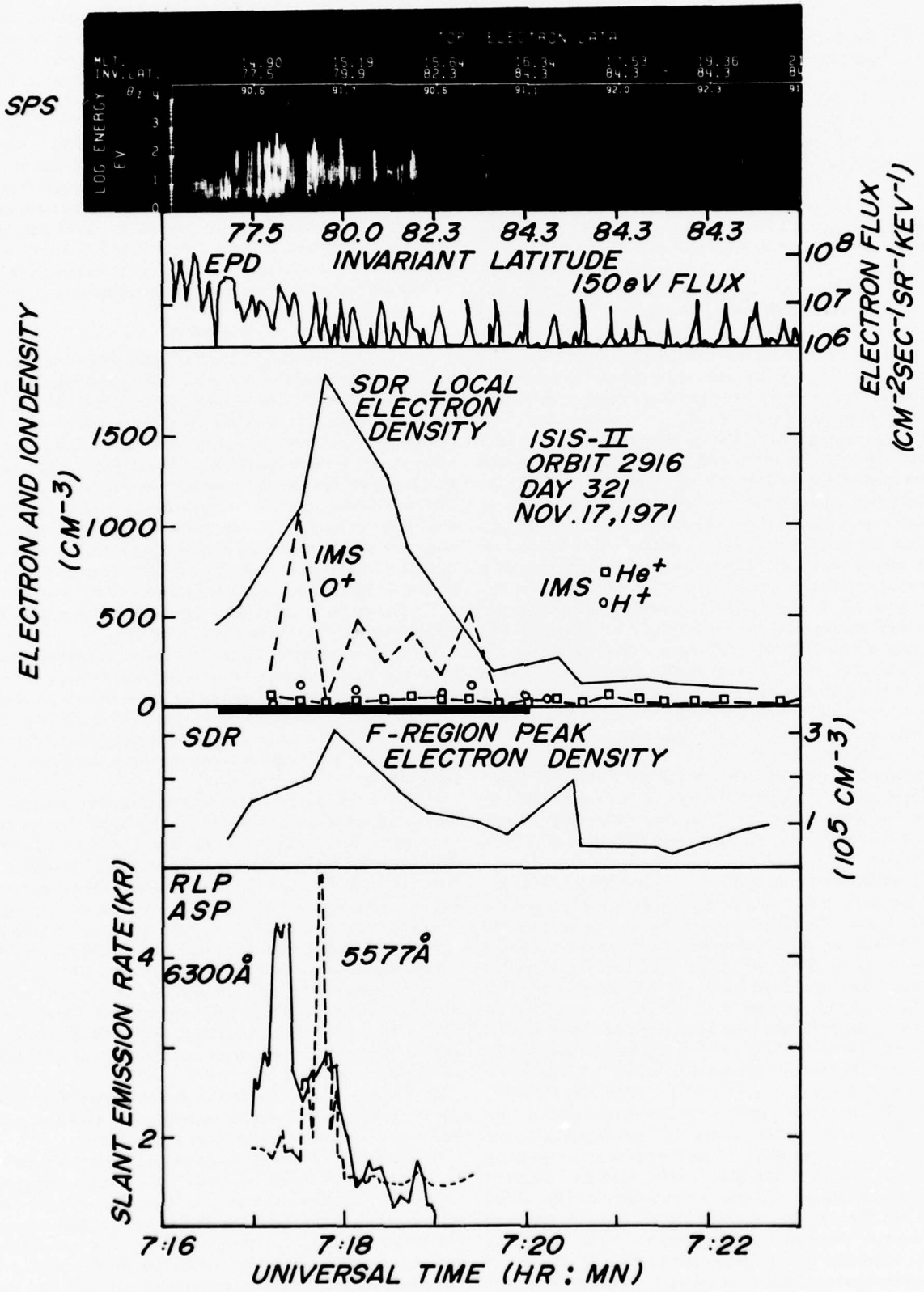

Fig. 8. Collected Isis 2 data for orbit 2916, November 17, 1971, at 15.0 hours MLT. The caption of Figure 2 is applicable.

DISCUSSION

All of the data shown here were obtained by relatively low levels of geophysical activity, from orbit 2916 (Kp = 0o) to 2928 (Kp = 2−), the other three having Kp values of 1−. The AE values order the orbits differently, from 2916 (AE = 20) to 2816 (AE = 79). However, for orbit 2928 (AE = 45) the AE value was 261 some 2 hours earlier, so some of the distinct characteristics of the pass may result from earlier substorm activity.

From the interplanetary magnetic field (IMF) data provided by *King* [1975] and *Fairfield and Ness* [1974] one finds that the interplanetary field turned from toward to away at 14 hours on November 8 and has remained so until late on November 10, which includes the first three orbits presented, 2816, 2827, and 2814. The following towards sector continued until November 22, which includes the last two orbits, 2928 and 2916. There are some data gaps in the intervals described, so the boundary crossings identified do not meet the criteria of *Wilcox et al.* [1975], but provided no rapid changes occurred, the identifications given here should be valid.

Thus the pronounced differences between the characteristics of the two groups of orbits and the consistency within each group suggest that the IMF influences the pattern of the cleft precipitation and the behavior of the cleft ionosphere. For the toward orbits the electron precipitation is of lower energy, exhibits less latitudinal structure extended over a broader region, and is located at a higher invariant latitude, extending poleward of 80°. (For orbit 2915, not described here, the flux extends to 83° invariant.) The data analyzed here are rather limited for such generalized conclusions, but *Titheridge* [1976] analyzed a very large body of topside ionosphere data and concluded that during toward sectors the cleft response is located at higher latitudes and is broader than during away sectors. For the away orbits described here the electron precipitation is confined to a narrow latitude region, is highly structured, and contains distinct regions of keV fluxes and 0.2-keV electrons. In two of the three cases the 0.2-keV precipitation was seen as narrow discrete flux regions on the poleward side of the keV precipitation, but in the other case a single intense 5- to 100-eV flux region appeared near the center of the keV flux region.

We consider now the differences in ionospheric behavior. For the away orbits the O^+ density measured at 1400 km closely follows the electron precipitation, showing its rapid upward diffusion above the region of production; it is also a region of strong upward H^+ polar wind flow. It may be that these cleft-associated flows are related to those observed in the plasma mantle [*Rosenbauer et al.*, 1975]. The O^+ disappears rapidly at the poleward boundary, implying the absence of poleward convection, or more likely, convective flow parallel to the cleft, the existence of which has been shown by *Heelis et al.* [1976] and by *Jeffries et al.* [1975]. In orbit 2814 the rise in ion temperature immediately at the poleward boundary supports this idea of minimal convection perpendicular to the oval. The appearance of He^+ as the dominant ion in the polar cap is consistent with the lack of polar wind flow observed there for these orbits. This may be characteristic of the winter polar cap. For the toward orbits the O^+ is clearly seen well poleward of the region of precipitation, consistent with a strong convective flow perpendicular to the oval. The rise in ion temperature also occurs considerably poleward of the precipitation region.

Another possibility is that the convective effects described are determined solely by proximity to local magnetic noon. This does not appear to be the case, because the times of 13.8 and 15.0 hours for the toward orbits overlap those of the away orbits at 14.1, 14.5, and 16.5 hours. On the other hand, if the effect of the IMF were to shift the convective pattern in local time, then a shift of about 1 hour would remove the overlap. This is consistent with the behavior described by *Heppner* [1972], where a dusk-to-dawn IMF (equivalent to toward) shifted the convective flow toward the afternoon side in the northern hemisphere. *Heelis et al.* [1976] have extended Heppner's one-dimensional dawn-dusk measurements by obtaining from the AE-C satellite two-dimensional ion flows near the cleft. They also find a tendency for the flow within the polar cap to be preferentially directed to either the morning side or the evening side in the five cases that they examined.

CONCLUSIONS

1. The electron energy spectrum varies dramatically over the latitude range of the cleft, with distinct components near 0.7 keV and 0.2 keV. The 0.7-keV components tend to be on the equatorward side, with narrow discrete 0.2-keV flux regions at the poleward boundary, but the 0.2-keV discrete regions can also be contained within the region of more energetic precipitation. The above pattern was observed during an IMF away sector, in which the region of cleft precipitation was also more confined in latitude and was below 80° invariant. During a toward sector the precipitating electrons were all close to 0.1 keV and formed a less structured pattern that was broader in latitude and extended poleward of 80° invariant.

2. The proton input is not a significant energy source for the ionospheric characteristics described here.

3. At 1400 km the O^+ density is enhanced to a few hundred ions per cubic centimeter over the region of cleft precipitation, and for an away sector it falls sharply at the poleward boundary. For a toward sector the O^+ was observed inside the polar cap, well beyond the region of electron energy input. These differences are attributed to convective flows parallel to and perpendicular to the auroral oval.

4. For some data points the electron densities measured by the topside sounder are a factor of 2 or 3 larger than the O^+ densities measured nearby. This may be due to the pronounced structure in the electron fluxes and the consequent ionospheric response to the charge input combined with the larger sampling volume of the sounder. In the one case of very high ionospheric densities the electron and ion densities were in agreement. The same ionospheric response may be responsible for the plasma waves detected by the RPA and CEP.

5. Throughout the region of cleft O^+ enhancement, polar wind flows of H^+ exceeding 1 km/s are observed. These terminate at the poleward cleft boundary, where the O^+ vanishes and He^+ becomes the dominant polar cap ion at 1400 km, about three times more abundant than H^+.

6. The ion temperature rises at the poleward cleft boundary when the perpendicular convective flow is weak and rises well beyond the boundary when the flow is rapid.

7. The 5577-Å and 6300-Å emissions are good indicators of the keV and eV fluxes, respectively. Frequently, a characteristic double hump structure is evident, the poleward one corresponding to the 0.2-keV electrons and the equatorward one having a red/green ratio nearer unity. But one optical peak can correspond to more than one electron flux peak, and additional weaker optical peaks are also observed. For the toward sector, with strong 0.1-keV fluxes, the red/green ratio reached a value of 8.

8. The F region peak density showed little response to the

cleft energy source, but in some cases a factor of 2 enhancement was discernible.

Acknowledgments. The authors are grateful to D. Boulding, spacecraft controller at the Communications Research Centre, Ottawa, and C. Freeman, data processing engineer at the Goddard Space Flight Center, for their part in acquiring and processing the data used here. This work is sponsored jointly by the Canadian Department of Communications and the National Aeronautics and Space Administration; direct support of some investigations is provided by the National Research Council of Canada. The University of Texas at Dallas portion of this work was supported by NASA grants NSG 5085 and 5087 and Air Force Geophysics Laboratory contract F19628-76-C-005.

The Editor thanks J. E. Titheridge for his assistance in evaluating this paper.

REFERENCES

Ahmed, M., and R. C. Sagalyn, Thermal positive ions in the dayside polar cusp measured on the Isis-1 satellite, *Space Res., 13*, 541, 1973.

Brace, L. H., and N. J. Miller, Ionospheric heating in the cleft (abstract), *Eos Trans. AGU, 55*, 69, 1974.

Dyson, P. L., and J. D. Winningham, Topside ionospheric spread *F* and particle precipitation in the dayside magnetospheric clefts, *J. Geophys. Res., 79*, 5219, 1974.

Fairfield, D. H., and N. F. Ness, Interplanetary sector structure: 1970–1972, *J. Geophys. Res., 79*, 5089, 1974.

Feldstein, Y. I., Some problems concerning the morphology of aurora and magnetic disturbances at high latitudes, *Geomagn. Aeron., 3*, 183, 1963.

Frank, L. A., and K. L. Ackerson, Observations of charged particle precipitation into the auroral zone, *J. Geophys. Res., 76*, 3612, 1971.

Heelis, R. A., W. B. Hanson, and J. L. Burch, Ion convection velocity reversals in the dayside cleft, *J. Geophys. Res., 81*, 3803, 1976.

Heikkila, W. J., The morphology of auroral particle precipitation, *Space Res., 12*, 1343, 1972.

Heikkila, W. J., and D. J. Winningham, Penetration of magnetosheath plasma to low altitudes through the dayside magnetospheric cusps, *J. Geophys. Res., 76*, 883, 1971.

Heppner, J. P., Polar cap electric field distributions related to the interplanetary magnetic field direction, *J. Geophys. Res., 77*, 4877, 1972.

Jeffries, R. A., W. H. Roach, E. W. Hones, E. M. Wescott, H. C. Stenbaek-Nielsen, T. N. Davis, and J. D. Winningham, Two barium plasma injections into the northern magnetospheric cleft, *Geophys. Res. Lett., 2*, 285, 1975.

King, J. H., Interplanetary magnetic field data 1963–74, *Rep. UAG-46*, World Data Center A for Solar-Terr. Phys., Boulder, Colo., 1975.

Knudsen, W. C., Magnetospheric convection and the high-latitude F_2 ionosphere, *J. Geophys. Res., 79*, 1046, 1974.

Knudsen, W. C., P. M. Banks, J. D. Winningham, and D. M. Klumpar, Theoretical modelling of the convecting F_2 ionosphere at high latitudes, paper presented at Sixteenth IUGG General Assembly, Grenoble, France, 1975.

Nishida, A., Average structure and storm time change of the polar topside ionosphere at sunspot minimum, *J. Geophys. Res., 72*, 6051, 1967.

Rosenbauer, H., H. Grünwaldt, M. D. Montgomery, G. Paschmann, and N. Sckopke, Heos 2 plasma observations in the distant polar magnetosphere: The plasma mantle, *J. Geophys. Res., 80*, 2723, 1975.

Sato, T., and L. Colin, Morphology of electron concentration at a height of 1000 km at polar latitudes, *J. Geophys. Res., 74*, 2193, 1969.

Shepherd, G. G., C. D. Anger, L. H. Brace, J. R. Burrows, W. J. Heikkila, J. Hoffman, E. J. Maier, and J. H. Whitteker, An observation of polar aurora and airglow from the Isis-2 spacecraft, *Planet. Space Sci., 21*, 819, 1973.

Shepherd, G. G., F. W. Thirkettle, and C. D. Anger, A topside optical view of the dayside cleft region, *Planet. Space Sci.*, in press, 1976.

Titheridge, J. E., Ionospheric heating beneath the magnetospheric cleft, *J. Geophys. Res., 81*, 3221, 1976.

Vasyliunas, V. M., Magnetospheric cleft symposium, *Eos Trans. AGU, 55*, 60, 1974.

Whalen, J. A., and C. P. Pike, *F* layer and 6300-Å measurements in the day sector of the auroral oval, *J. Geophys. Res., 78*, 3848, 1973.

Whitteker, J. H., The magnetospheric cleft—Ionospheric effects, *J. Geophys. Res., 81*, 1279, 1976.

Wilcox, J. M., L. Svalgaard, and P. C. Hedgecock, Comparison of inferred and observed interplanetary magnetic field polarities, 1970–1972, *J. Geophys. Res., 80*, 3685, 1975.

(Received May 27, 1976;
accepted July 28, 1976.)

VOL. 81, NO. 4 JOURNAL OF GEOPHYSICAL RESEARCH FEBRUARY 1, 1976

Dependence of the Latitude of the Cleft on the Interplanetary Magnetic Field and Substorm Activity

Y. KAMIDE,[1,2,3] J. L. BURCH,[4] J. D. WINNINGHAM,[5] AND S.-I. AKASOFU[1]

The latitudinal motion of the cleft (the polar cusp) associated with the southward interplanetary magnetic field (IMF) and substorm activity is examined. The cleft location is identified on the basis of the location of midday auroras and of electron precipitation (Ogo 4 and Isis 1 satellites). It is found that the IMF and substorm activity control independently the latitude of the cleft and that they can shift the cleft location by 3°–4° under average conditions.

Several workers have presented clear evidence which indicates that there occurs an inward motion of the magnetopause and the accompanying equatorward shift of the cleft (the polar cusp) during periods when the interplanetary magnetic field (IMF) has a southward component [*Fairfield*, 1971; *Russell et al.*, 1971; *Burch*, 1972, 1973; *Yasuhara et al.*, 1973; *Maezawa*, 1974; *Pike et al.*, 1974; and many others]. *Aubry et al.* [1970] showed that following a southward turning of the IMF at about 1730 UT on March 27, 1968, the magnetopause distance became smaller than that expected from the observed dynamical pressure of the solar wind. *Maezawa* [1974] confirmed statistically the dependence of the magnetopause position on the polarity of the IMF, after eliminating the possible effect of the solar wind pressure variations. *Fairfield and Ness* [1970], *Meng et al.* [1971], *Nishida and Nagayama* [1973], *Caan et al.* [1973], and *Meng and Colburn* [1974] have established that a southward IMF is followed by an increase of the magnetic energy density in the lobes of the tail. Theoretical interpretations of these observations have been given by *Coroniti and Kennel* [1973] and *Kan and Akasofu* [1974].

On the other hand, *Patel and Dessler* [1966] and *Meng* [1970] showed that the magnetopause distance varies with geomagnetic activity as well. Further, the equatorward shift of the day side auroral oval and the cleft has been found to be correlated with an increase of geomagnetic activity indices [*Feldstein and Starkov*, 1967; *Burch*, 1970; *Chubb and Hicks*, 1970; *Winningham*, 1972; *McDiarmid et al.*, 1972]. *Akasofu* [1972*a*] and *Snyder et al.* [1973] have shown that midday auroras and the ionospheric *F* layer irregularity zone move equatorward (and poleward) simultaneously with the development (and the decay) of substorms in the night sector.

It is thus of great interest to examine whether or not the location of the cleft depends only on the north-south component of the IMF or on both the IMF and the substorm activity. If the latter is the case, it is important to examine quantitatively both dependences. The earlier studies cited above are not conclusive in examining these problems. *Burch* [1972] showed that the boundary of the 'soft' precipitation zone (cleft) moves equatorward during periods of the southward IMF even without significant substorm activity. He suggested then that the IMF is more important than substorm activity in controlling the cleft location, although he noted also that the scatter in his result might arise from substorm effects [*Burch*, 1974].

As a first step in examining this problem we examined the equatorward shift of midday auroras over the South Pole station (−78.5°, 360.0° in geomagnetic coordinates) which occurred during periods of a reasonably steady IMF condition. An example is shown in Figure 1; for details of the all-sky camera installed at the South Pole station see *Akasofu* [1972*a*]. Dipole noon at this station is about 1600 UT.

Figure 1 shows, from the top, the magnitude and the B_z component (in solar magnetospheric (SM) coordinates) of the IMF, the superposed *H* component magnetic records along the auroral zone in the dark sector, and the approximate location of the midday auroral arc which is located nearest to the equator. The height of the aurora was assumed to be 130 km. The hourly *Dst* values are also shown. Note that the traveling time of the interplanetary signal to the earth is approximately 7 min if the solar wind speed is assumed to be 400 km/s.

The superposition of the *H* component traces indicates that the first substorm took place when the IMF B_z was fluctuating around the value of −4 γ. The onset time of the substorm was at about 1500 UT at the latest. At about the same time a fairly bright arc began to move equatorward over the South Pole. After 1530 UT, the westward electrojet (the negative *H* bay) subsided very quickly. Coincident with this, the arc began to shift back poleward. From 1640 UT the electrojet activity was enhanced gradually until about 1900 UT. During this interval an arc appeared near the poleward horizon and moved equatorward. When the auroral electrojet was intensified at about 1930 UT, the arc left the field of view of the all-sky camera and reappeared at 2040 UT. The intensity of the IMF southward component gradually decreased between 1700 and 2000 UT.

The equatorward shift of the midday aurora in this particular sequence of events is thus much more closely related to substorm activity than IMF changes, since the IMF B_z component did not show any definite change during the first substorm and even decreased during the second substorm. Thus it is of great interest to extend Burch's study in examining whether or not the IMF and substorm activity control independently the cleft location.

OGO 4 AND ISIS 1 DATA

Burch [1973] showed that the cleft location can be determined mainly by the intensity and duration of the IMF southward component. He demonstrated that the 45-min average value of the interplanetary B_z predicts best the latitudes of the

[1] Geophysical Institute, University of Alaska, Fairbanks, Alaska 99701.
[2] Cooperative Institute for Research in Environmental Sciences, University of Colorado, Boulder, Colorado 80302.
[3] Guestworker at Data Studies Division, NOAA/EDS/NGSDC, Boulder, Colorado 80302.
[4] Magnetospheric and Plasma Physics Branch, NASA Marshall Space Flight Center, Huntsville, Alabama 35812.
[5] Institute of Physical Sciences, University of Texas at Dallas, Richardson, Texas 75080.

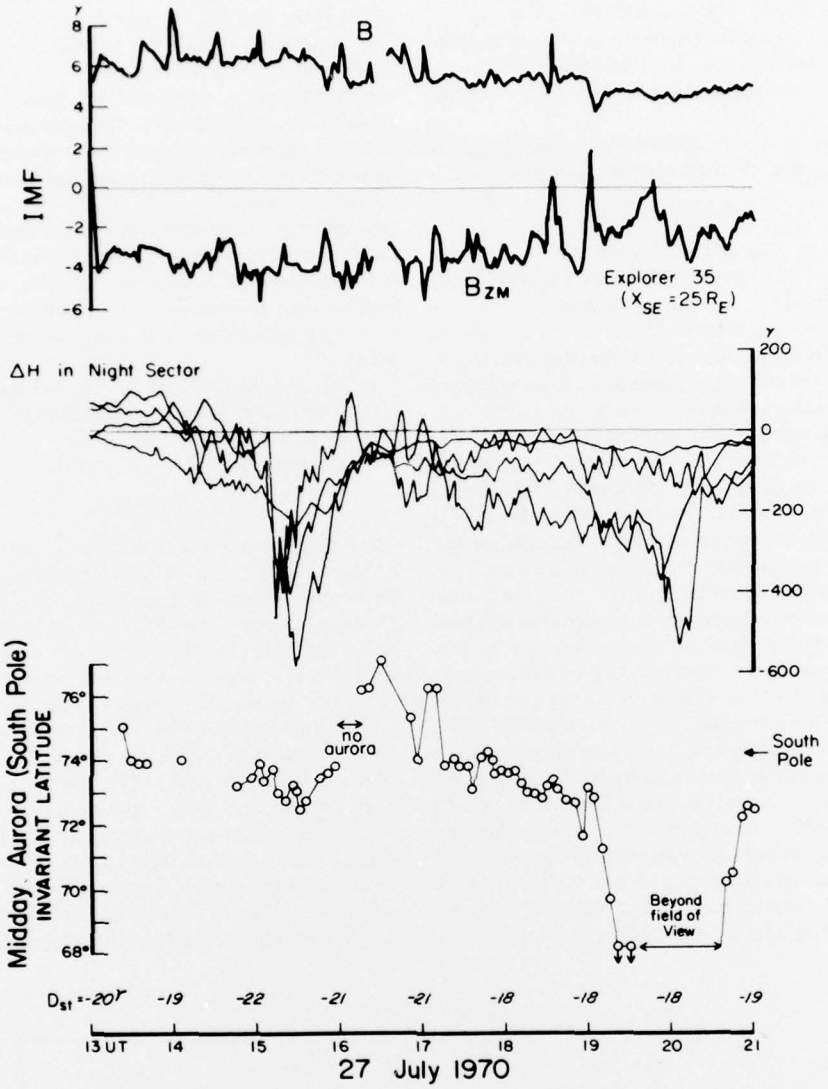

Fig. 1. The IMF (magnitude and B_z component), the superposed H component magnetic records from four auroral zone stations in the dark sector (Dixon Island, Cape Chelyuskin, Tixie Bay, and Cape Wellen), and the location of the midday aurora observed at the South Pole station on July 27, 1970. The *Dst* index is also shown.

poleward and equatorward boundaries of cleft with rms errors of 1.34° and 1.16°, respectively. He has found also that the cleft latitudes were ordered much better using the B_z value rather than the θ (the latitude angle of the IMF). The purpose of this section is to investigate further the accuracy with which the cleft location can be predicted based on the IMF and the available geomagnetic activity indices.

Data. Full information concerning the Ogo 4 (altitude 400–900 km) auroral particle experiment and the electron data used in determining the cleft is given by ***Hoffman and Evans*** [1968] and ***Burch*** [1973], respectively. From July to October in 1967 and 1968, 54 Ogo 4 passes were chosen, which occurred in the 0900–1500 magnetic local time (MLT) sector. The delay time from the interplanetary observing position to the magnetopause was less than 5 min. The invariant latitude of the cleft was determined on the basis of electron data of energies 0.7, 2.3 and 7.3 keV. Throughout this study we restrict our attention to the lower (equatorward) boundary of the cleft. This is because for the upper boundary (1) it is more difficult to make unambiguous identification of the precipitation boundary in many cases, owing to the appearance of localized spikes or drizzle of precipitation into the polar cap [***Winningham and Heikkila,*** 1974], (2) the data sample number (21 samples) is too small, and (3) the fact that all the 12 passes for the southward IMF took place during substorms makes separation of the IMF and substorm effects impossible.

Details of the Isis 1 soft particle spectrometer can be found in the work by ***Heikkila et al.*** [1970]. The method deriving the cleft boundary can be found in the work by ***Yasuhara et al.*** [1973]. Data included in this paper were obtained between February and July in 1969 in the 0800–1600 MLT period.

The IMF data used here are recorded by Explorer 34 and Explorer 35 for the Ogo 4 and Isis 1 data, respectively. To determine the delay time of the interplanetary signal to the magnetopause (which was assumed to be at $X_{SM} = 10\ R_E$) in each case, available solar wind velocity measurements from

Explorer 33, 34, or 35 were used. Substorm activity was mainly monitored by the *AE* index [*Allen et al.*, 1973, 1974*a*, *b*].

Results. Figure 2 shows the relationship between the cleft location (the lower latitude boundary) and the IMF B_z component averaged for periods of 45 min prior to the satellite passes.

The dashed curve in Figure 2 shows the relationship between the cleft latitude Λ (in degrees) and B_z (in gammas)

$$\Lambda = 75.5 + 0.53B_z - 0.05B_z^2$$

which was obtained by a least squares quadratic fit to the data; the rms deviation is 1.16° [*Burch*, 1973]. This empirical equation predicts the latitude of the equatorward boundary of the cleft with an accuracy of better than 3° for $-6\,\gamma < B_z < 6\,\gamma$. It can be seen that a systematic lowering of the cusp of about 5° occurs between $B_z = 0$ and $-6\,\gamma$, whereas it moves poleward by only 1.5° for positive values up to $+6\,\gamma$.

The points are grouped into quiet periods by open circles and substorm times by triangles. The division between the quiet and the substorm cases was made primarily by referring to the presence of a sharp increase of the *AE* index (i.e., a decrease in the *H* component along the night side auroral zone). We also checked carefully individual magnetograms in auroral latitudes and mid-latitudes. For the five points, however, it was not possible to determine from the available geomagnetic records whether there occurred substorms or just fluctuations. These points are represented by double circles in Figures 2 and 3. It is clear that almost all the points observed during substorms lie below the dashed curve, regardless of the polarity of the IMF. In contrast, it is seen that the cleft during quiet times is located at higher latitudes than the above empirical equation predicts. The cleft during substorms associated with the northward IMF is located almost at the same latitude as it is during geomagnetically quiet period with the southward IMF. This feature can be seen particularly in the range of $-3 \le B_z \le 2\,\gamma$, where the sample number for quiet times is almost the same as that for substorm times. Exceptions (marked by points A and B in Figures 2 and 3) occurred under unusual states of the IMF. The point A was observed during an abnormally large magnitude of the IMF ($\sim 18\,\gamma$), so that the corresponding θ_{SM} value of the IMF was only $-19°$. The point B actually occurred during a northward IMF time, although the average B_z value for 45 min prior to the satellite pass was $-2.43\,\gamma$; a sudden northward turning of the IMF occurred about 20 min before the Ogo 4 pass. Both were observed during rather small substorms (maximum $|AL| = 280$ and $310\,\gamma$ for A and B, respectively). These characteristic features indicate that both the IMF and the substorm activity are related to the location of the equatorward boundary of the cleft. A similar tendency is found in the published data of electron and proton cleft precipitation as determined from Isis 1 satellite [*Yasuhara et al.*, 1973].

In Figure 3 the difference $\Delta\Lambda$ between the invariant latitudes of the observed cleft and the latitude expected purely from the average B_z of the IMF are plotted as a function of three geomagnetic indices (*AE*, *Kp*, and *Dst*):

$$\Delta\Lambda = \Lambda_{obs} - \Lambda_o$$

where Λ_{obs} is the actual observed latitude and $\Lambda_o = 75.5 + 0.53B_z - 0.05B_z^2$. Generally, $\Delta\Lambda$ becomes more negative with the increase of geomagnetic activity. It correlates well with the *AE* index, except for the points A and B; the abnormal behavior of the IMF at those times was described earlier. It is surprising that even the *Kp* index, which is a 3-hour interval index, can predict the deviation of the cleft latitude from the level that is expected from the IMF B_z alone. It should be noted that there is a close relationship between the B_z of the IMF and the *AE* [*Arnoldy*, 1971; *Meng et al.*, 1973], *Kp* [*Hirshberg and Colburn*, 1969], and *Dst* [*Kane*, 1974; *Kamide*, 1974] indices. Thus it is not particularly surprising that the cleft location depends on all these indices.

Further, an attempt was made to determine statistical equatorward boundary of the cleft on the basis of the two parameters, B_z and *AE*. Measurements from polar-orbiting satellites,

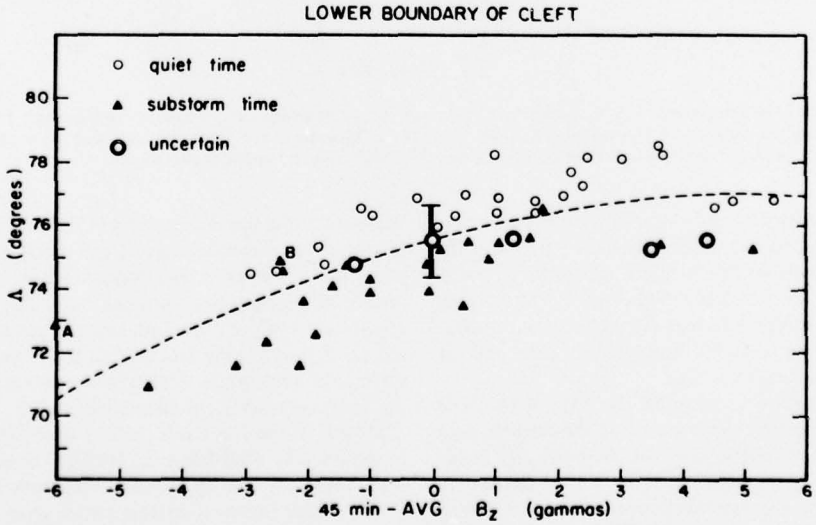

Fig. 2. Location of the equatorward boundary Λ of day side (0900–1500 hours MLT) cleft electron precipitation (based on Ogo 4 data) for 45-min B_z averages between -6 and $+6\,\gamma$. The dashed curve represents a second-order polynomial fit to to the data; $\Lambda = 75.5 + 0.53B_z - 0.05B_z^2$. The points are grouped into quiet periods and substorm times depending on the magnetic condition of the period when the left was observed. For an explanation of points A and B see the text.

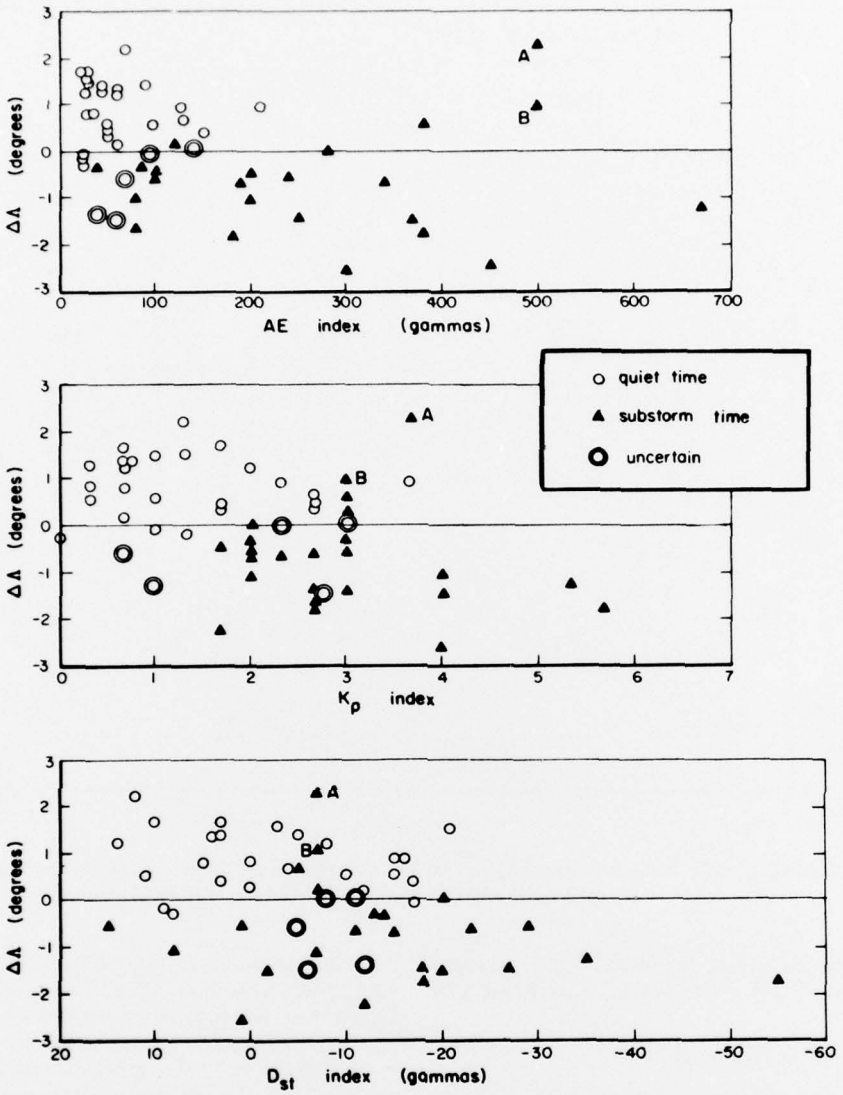

Fig. 3. Dependence of ΔΛ (the difference between the invariant latitude of the observed cleft and the latitude expected purely from the average B_z) on three geomagnetic activity indices (*AE*, *Kp*, and *Dst*).

however, have an inherent drawback in that the determination of the cleft position is obtained only once per orbit in the northern hemisphere. To overcome this difficulty, we have added 63 points of the cleft precipitation boundary determined from Isis 1 satellite data. One must be cautious in combining the two sets of data (Ogo 4 and Isis 1), since the boundary determined by detectors for particles of different energies may have a slightly different meaning. Also, some error could emerge from the determination of the 45-min average B_z value, since the interplanetary satellite (Explorer 33) was behind the earth ($X_{SM} = -10$ to -87 R_E) during the measurements by Isis 1 in 1969.

The results are shown in Figure 4 by drawing the lines of equal latitudes Λ of the cleft location by a computer after plotting the observed values Λ on the B_z-*AE* diagram. The scale of the horizontal line (B_z of the IMF) and the vertical scale (*AE* index value) are given in such a way that the range of the B_z value (14.9 $\gamma = B_{z\,max} - B_{z\,min}$) for the 117 cases, that we have examined here, and the maximum *AE* value (900 γ) are represented with the same length. If the B_z value is the only important factor in determining the cleft location regardless of substorm activity, these isolatitude lines should be vertical. It can be seen from this statistical result that both the IMF and the substorm activity have a determining role for the latitude of the cleft and that both have about the same amount of influence in terms of the latitudinal shift in the range which we have examined in this study (especially for the B_z range less than $+3$ γ). There is also a tendency that for the northward IMF ($B_z > +3$ γ) the cleft motion is more sensitive to the *AE* index than for $B_z < +3$ γ. This is reflected in the lack of strong dependence on the IMF as it becomes more northward, resulting in a behavior dominated by the level of substorm activity. One should note, however, that the *AE* index is not most suitable for monitoring properly 'contracted oval substorms,'

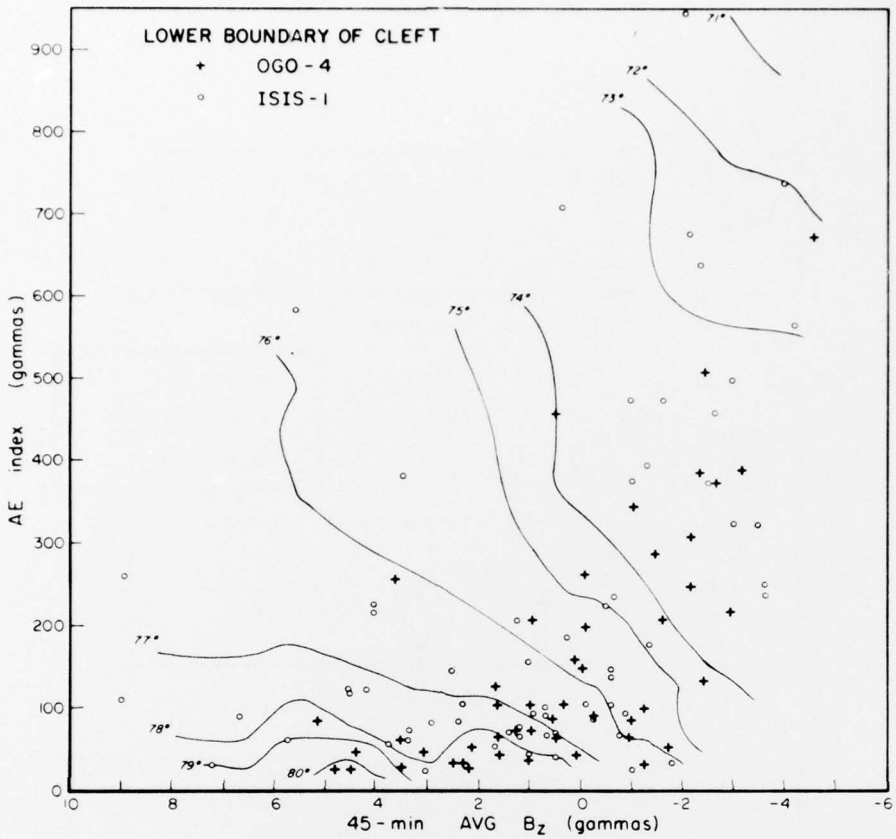

Fig. 4. Equivalue (of the latitude of the cleft) contours as functions of the 45-min average B_z and the AE index, constructed on the basis of 117 observed values by the Ogo 4 and the Isis 1 satellites.

which occur beyond the field of view of the AE stations generally under northward IMF conditions [cf. *Kamide and Akasofu*, 1974].

Discussion

In this study we have identified the separate roles of the IMF and substorm activity in controlling the latitude of the equatorward boundary of cleft electron precipitation. Although periods of strong southward IMF have been observed to be associated with very low latitude cleft locations even during quiet times, the occurrence of substorms has been shown here to add noticeably to this equatorward shift. Added to knowledge of the interplanetary B_z component, a simple classification into quiet or substorm conditions improves considerably the accuracy with which the cleft latitude can be predicted.

The role of the southward IMF to initiate the net transfer of magnetic flux from the day side to the night side which is associated with the equatorward shift of the cleft has been discussed in the literature [e.g., *Coroniti and Kennel*, 1973; *Kan and Akasofu*, 1974; *Burch*, 1973]. It is thus reasonable to infer that the efficiency of transfer of day side magnetic flux depends on the amount of the southward IMF flux impinging on the magnetosphere, which is proportional to the dawn-dusk electric field across the polar cap [e.g., *Sonnerup*, 1974].

The present study indicates that the occurrence of magnetospheric substorms also influences greatly the cleft location. Such a relationship between the cleft location and the AE may not be unexpected, since there appears to be a general relationship between the southward IMF and the AE index [cf. *Arnoldy*, 1971; *Meng et al.*, 1973]. This paper, however, stresses that the cleft moves equatorward in conjunction with the occurrence of substorms even during a northward IMF period. It is also shown that, even during extended periods of nearly constant IMF, the substorm effects are particularly apparent such that time variations of the equatorward shift of the midday aurora and those of the auroral electrojet in the midnight sector are very similar (see Figure 1).

It has generally been thought that the magnetospheric substorm is a manifestation of a suddenly enhanced reconnection of magnetic flux in the magnetotail, returning the newly closed fluxes to the day side. Thus we would expect a poleward motion of the cleft during substorms. *Akasofu* [1972*a*] showed, however, that the equatorward drift of the cleft is well correlated with a growth of negative bays along the auroral zone in the midnight sector and that the subsequent poleward return of the cleft is correlated with the recovery of the negative bays. Thus the observed equatorward motion of the cleft does not seem to agree with the above-mentioned concept of the substorm.

There are at least two possibilities for this conflict. The first one is that during a substorm there occurs a process which causes an equatorward motion of the cleft. *Yasuhara et al.* [1975*a*] have recently shown that an enhancement of the S_q^P (three-dimensional) current system during substorms can shift the cleft location equatorward by a few degrees. The S_q^P current system consists of a flow into the morning part of the

auroral oval along magnetic field lines, along the auroral oval, and out from the evening part of the oval along field lines. The growth of such a current system during substorms was first proposed by *Akasofu* [1972*b*], and has been discussed by *McPherron et al.* [1973], *Kamide et al.* [1974], and *Kawasaki et al.* [1974]. Indeed, *Yasuhara et al.* [1975*b*] showed, on the basis of their analysis of Triad data, that the intensity of field-aligned currents increases with *Kp*.

The second possibility is that the cleft location does not indicate the demarcation line between the open and closed fluxes during substorms and thus that the equatorward cleft motion does not indicate the net transfer of magnetic flux from the day side magnetosphere to the magnetotail. Indeed, it is not necessarily certain, at present, whether or not the cleft precipitation always occurs near the boundary of the open and closed field lines. *McDiarmid et al.* [1972] showed that the cleft precipitation can occur well equatorward of the trapping boundary. It is suggested that the location of the cleft precipitation with respect to the trapping boundary should be examined as a function of substorm activity. It is of great interest to examine how the equatorward boundary of the area of the precipitation of solar electrons varies during a substorm, since low-energy solar electrons are thought to be good traces of magnetic field lines.

Acknowledgments. We thank R. A. Hoffman for providing Ogo 4 data. Valuable discussions with J. R. Kan, F. Yasuhara, and J. Horwitz are gratefully acknowledged. This work was supported in part by National Science Foundation grants, GA-37094 and DES-74-23832, to the Geophysical Institute, University of Alaska. The University of Texas at Dallas portion of this work was supported by AFCRL contract F 19628-75-C-0032 and NASA grant NGR 44-044-150.

The Editor thanks K. Maezawa for his assistance in evaluating this report.

REFERENCES

Akasofu, S.-I., Midday auroras at the south pole during magnetospheric substorms, *J. Geophys. Res.*, *77*, 2303, 1972*a*.

Akasofu, S.-I., Magnetospheric substorms: A model, in *Solar Terrestrial Physics*, edited by E. R. Dyer, pp. 131–151, D. Reidel, Dordrecht, Netherlands, 1972*b*.

Allen, J. H., C. C. Abston, and L. D. Morris, Auroral electrojet magnetic activity indices *AE*(11) for 1968, *Rep. UAG-29*, World Data Center A for Solar Terr. Phys., NOAA, Boulder, Colo., 1973.

Allen, J. H., C. C. Abston, and L. D. Morris, Auroral electrojet magnetic activity indices *AE*(11) for 1969, *Rep. UAG-31*, World Data Center A for Solar Terr. Phys., NOAA, Boulder, Colo., 1974*a*.

Allen, J. H., C. C. Abston, and L. D. Morris, Auroral electrojet magnetic activity indices *AE*(10) for 1967, *Rep. UAG-33*, World Data Center A for Solar Terr. Phys., NOAA, Boulder, Colo., 1974*b*.

Arnoldy, R. L., Signature in the interplanetary medium for substorms, *J. Geophys. Res.*, *76*, 5189, 1971.

Aubry, M. P., C. T. Russell, and M. G. Kivelson, On inward motion of the magnetopause preceding a substorm, *J. Geophys. Res.*, *75*, 7018, 1970.

Burch, J. L., Satellite measurements of low energy electrons precipitated at high latitudes, in *The Polar Ionosphere and Magnetospheric Processes*, edited by G. Skovli, pp. 67–78, Gordon and Breach, New York, 1970.

Burch, J. L., Precipitation of low-energy electrons at high latitudes: Effects of interplanetary magnetic field and dipole tilt angle, *J. Geophys. Res.*, *77*, 6696, 1972.

Burch, J. L., Rate of erosion of day side magnetic flux based on a quantitative study of the dependence of polar cusp latitude on the interplanetary magnetic field, *Radio Sci.*, *8*, 955, 1973.

Burch, J. L., Observations of interactions between interplanetary and geomagnetic fields, *Rev. Geophys. Space Phys.*, *12*, 363, 1974.

Caan, M. N., R. L. McPherron, and C. T. Russell, Solar wind and substorm-related changes in the lobes of the geomagnetic tail, *J. Geophys. Res.*, *78*, 8087, 1973.

Chubb, T. A., and G. T. Hicks, Observations of the aurora in the far ultraviolet from Ogo 4, *J. Geophys. Res.*, *75*, 1290, 1970.

Coroniti, F. V., and C. F. Kennel, Can the ionosphere regulate magnetospheric convection?, *J. Geophys. Res.*, *78*, 2837, 1973.

Fairfield, D. H., Average and unusual locations of the earth's magnetopause and bow shock, *J. Geophys. Res.*, *76*, 6700, 1971.

Fairfield, D. H., and N. F. Ness, Configuration of the geomagnetic tail during substorms, *J. Geophys. Res.*, *75*, 7032, 1970.

Feldstein, Y. I., and G. V. Starkov, Dynamics of auroral belt and polar geomagnetic disturbances, *Planet. Space Sci.*, *15*, 209, 1967.

Heikkila, W. J., J. B. Smith, J. Tarstrup, and J. D. Winningham, The soft particle spectrometer in the Isis 1 satellite, *Rev. Sci. Instrum.*, *4*, 1393, 1970.

Hirshberg, J., and D. S. Colburn, Interplanetary field and geomagnetic variations—A unified view, *Planet. Space Sci.*, *17*, 1183, 1969.

Hoffman, R. A., and D. S. Evans, Field-aligned electron bursts at high latitudes observed by Ogo 4, *J. Geophys. Res.*, *73*, 6201, 1968.

Kamide, Y., Association of *DP* and *DR* fields with the interplanetary magnetic field variation, *J. Geophys. Res.*, *79*, 49, 1974.

Kamide, Y., and S.-I. Akasofu, Latitudinal cross section of the auroral electrojet and its relation to the interplanetary magnetic field polarity, *J. Geophys. Res.*, *79*, 3755, 1974.

Kamide, Y., F. Yasuhara, and S.-I. Akasofu, On the cause of northward magnetic field along the negative x-axis during magnetospheric substorms, *Planet. Space Sci.*, *22*, 1219, 1974.

Kan, J. R., and S.-I. Akasofu, A model of the open magnetosphere, *J. Geophys. Res.*, *79*, 1379, 1974.

Kane, R. P., Relationship between interplanetary plasma parameters and geomagnetic *Dst*, *J. Geophys. Res.*, *79*, 64, 1974.

Kawasaki, K., C.-I. Meng, and Y. Kamide, The development of three-dimensional current system during a magnetospheric substorm, *Planet. Space Sci.*, *22*, 1471, 1974.

Maezawa, K., Dependence of the magnetopause position on the southward interplanetary magnetic field, *Planet. Space Sci.*, *22*, 1443, 1974.

McDiarmid, I. B., J. R. Burrows, and M. D. Wilson, Solar particles and the day side limit of closed field lines, *J. Geophys. Res.*, *77*, 1103, 1972.

McPherron, R. L., C. T. Russell, and M. P. Aubry, Satellite studies of magnetospheric substorms on August 15, 1968, 9, Phenomenological model of substorms, *J. Geophys. Res.*, *78*, 3131, 1973.

Meng, C.-I., Variations of the magnetopause position with substorm activity, *J. Geophys. Res.*, *75*, 3252, 1970.

Meng, C.-I., and D. S. Colburn, Magnetotail variations associated with the southward interplanetary magnetic field, *J. Geophys. Res.*, *79*, 1831, 1974.

Meng, C.-I., S.-I. Akasofu, E. W. Hones, and K. Kawasaki, Magnetospheric substorms in the distant magnetotail observed by Imp 3, *J. Geophys. Res.*, *76*, 7584, 1971.

Meng, C.-I., B. Tsurutani, K. Kawasaki, and S.-I. Akasofu, Cross-correlation analysis of the *AE* index and the interplanetary magnetic field B_z component, *J. Geophys. Res.*, *78*, 617, 1973.

Nishida, A., and N. Nagayama, Magnetotail response to sudden changes in the interplanetary magnetic field, *Astrophys. Space Sci.*, *20*, 459, 1973.

Patel, V. L., and A. J. Dessler, Geomagnetic activity and size of magnetospheric cavity, *J. Geophys. Res.*, *71*, 1940, 1966.

Pike, C. P., C.-I. Meng, S.-I. Akasofu, and J. A. Whalen, Observed correlations between interplanetary magnetic field variations and the dynamics of the auroral oval and the high-latitude ionosphere, *J. Geophys. Res.*, *79*, 5129, 1974.

Russell, C. T., C. R. Chappell, M. D. Montgomery, M. Neugebauer, and F. L. Scarf, Ogo 5 observations of the polar cusp on November 1, 1968, *J. Geophys. Res.*, *76*, 6743, 1971.

Snyder, A. L., S.-I. Akasofu, and C. P. Pike, The day-sector polar *F*-layer during a magnetospheric substorm, *Planet. Space Sci.*, *21*, 399, 1973.

Sonnerup, B. U. Ö., Magnetopause reconnection rate, *J. Geophys. Res.*, *79*, 1546, 1974.

Winningham, J. D., Characteristics of magnetosheath plasma observed at low altitudes in the dayside magnetospheric cusps, in *Earth's Magnetospheric Processes*, edited by B. M. McCormac, pp. 68–80, D. Reidel, Dordrecht, Netherlands, 1972.

Winningham, I. D., and W. J. Heikkila, Polar cap auroral electron fluxes observed with Isis 1, *J. Geophys. Res.*, *79*, 949, 1974.

Yasuhara, F., S.-I. Akasofu, J. D. Winningham, and W. J. Heikkila, The equatorward shift of the cleft during magnetospheric substorms as observed by Isis 1, *J. Geophys. Res., 78,* 7286, 1973.

Yasuhara, F., Y. Kamide, and S.-I. Akasofu, A modeling of the magnetospheric substorm, *Planet. Space Sci., 23,* 575, 1975*a*.

Yasuhara, F., Y. Kamide, and S.-I. Akasofu, Field-aligned and ionospheric currents, *Planet. Space Sci., 23,* in press, 1975*b*.

(Received May 9, 1975;
accepted July 30, 1975.)

VOL. 82, NO. 1 JOURNAL OF GEOPHYSICAL RESEARCH JANUARY 1, 1977

Ionosonde Observations of the Northern Magnetospheric Cleft During December 1974 and January 1975

G. S. STILES,[1] E. W. HONES, JR.,[2] J. D. WINNINGHAM,[3] R. P. LEPPING,[4] AND B. S. DELANA[5]

During December 1974 and January 1975 the northern magnetospheric cleft was monitored by ionosondes at Cape Parry and Sachs Harbor, Northwest Territories, Canada, in support of rocket shots into the cleft. Ionograms were taken nominally at 15-min intervals but as rapidly as two per minute during times of particular interest. Analysis of 5 days of data shows the ionosphere at cleft latitudes to be very complex and dynamic. The ionograms often show considerable structure and can change appearance significantly in a minute or two. The cleft at times appears to move equatorward in response either to a southward turning of the interplanetary magnetic field or to the occurrence of geomagnetic disturbances. This response is in agreement with the conclusions of previous satellite studies. Behavior contrary to this generalization is not uncommon, however, and therefore it may not always hold on time scales considerably shorter than the satellite orbital period of $\gtrsim 1$ hour. The rate of the cleft's motion may vary from ~ 0.05 to ~ 0.5 deg/min.

INTRODUCTION

Since the initial discovery of the magnetospheric cleft by satellite instrumentation [*Heikkila et al.*, 1970; *Winningham*, 1970; *Heikkila and Winningham*, 1971; *Frank*, 1971; *Frank and Ackerson*, 1971; *Russell et al.*, 1971], considerable effort has been devoted to the investigation of this phenomenon (see the summary by *Vasyliunas* [1974]). This work has shown that the plasma found in the cleft is very much like that seen in the magnetosheath [e.g., *Winningham*, 1972]. The location of the cleft has been found to respond both to changes in the interplanetary magnetic field and to the occurrence of geomagnetic disturbances [*Burch*, 1972; *Kamide et al.*, 1976]. Much of the current study in this field is thus devoted to the relation between the interplanetary and cleft magnetic fields and the mechanism by which the magnetosheath plasma enters the cleft.

During December 1974 and January 1975 two groups launched rockets into the northern cleft in attempts to examine the particle populations, the magnetic field, and the convection of plasma. The success of these experiments depended upon an accurate knowledge of the location of the cleft prior to the launching of the rockets. Ground-based ionosondes were one of the techniques used to monitor the cleft's position. In this paper we describe the results of an analysis of the ionograms made in support of the rocket flights.

The rockets were launched from Cape Parry, located on the Arctic coast of Canada (Figure 1). The December flights were organized by a Canadian group and concentrated on making optical and particle measurements; the initial results are reported by *Shepherd et al.* [1976]. The January flights were a cooperative effort by the Los Alamos Scientific Laboratory (LASL) and the University of Alaska (UAK). Two rockets were launched whose primary purpose was to project barium ion clouds upward along the cleft field lines by means of shaped explosive charges. The rockets also carried particle detectors. The LASL-UAK experiments have been described by *Jeffries et al.* [1975].

A considerable amount of ground based data were taken in support of these flights to aid both in the location of the cleft and in the interpretation of the results. Ionosondes were located at Cape Parry and Sachs Harbor (see Figure 1). Ionosondes have proven most useful in locating the projection of the cleft upon the ionosphere [*Pike*, 1971, 1972; *Winningham and Pike*, 1972; *Pike et al.*, 1974; *Ungstrup et al.*, 1975; *Shepherd et al.*, 1976]. Ionograms were taken nominally at 15-min intervals; however, during periods of particular interest the spacing was decreased to a minute or so.

Optical phenomena were also monitored. Photometers were installed at Cape Parry and Sachs Harbor, and an all-sky camera was located at Sachs Harbor. Some of the photometric observations during this period are described by *Shepherd et al.* [1976]. *Whalen and Pike* [1973] had shown earlier that photometer measurements of 6300-Å emissions may be used to determine the position of the cleft.

Satellite data were used to check the ground-based measurements and to aid in the analysis of the results. The position of the cleft was measured on several passes by the soft particle spectrometer (SPS) aboard Isis 2 [*Heikkila and Winningham*, 1971]. Defense Meteorological Satellite Program satellite photos [e.g., *Pike and Whalen*, 1974] were used to monitor auroral activity. The interplanetary magnetic field (IMF) and solar wind velocity were measured by Imp 8 whenever that satellite was suitably located. One of the principal goals of the present study was to investigate the relation between changes in the IMF and the movement of the cleft. Earlier work [e.g., *Burch*, 1972] indicates that the motion of the cleft is correlated with changes in the z component of the IMF.

RESULTS

Since the ionospheric manifestation of the cleft may be a degree or more wide and since its poleward boundary may not be sharply defined, ionosondes are most useful in tracking the position of the cleft when it is poleward of the sounder. Under these conditions, oblique echoes of the ionosonde radio signals from the cleft's relatively sharp equatorward boundary of ionization will produce unique traces on the ionogram provided that the cleft is not too distant (examples are given by *Pike* [1971, 1972], *Pike et al.* [1974], *Ungstrup et al.* [1975], and *Shepherd et al.* [1976]). During the December and January period this condition was satisfied for 5 of the 7 days on which

[1] Center for Research in Aeronomy, Utah State University, Logan, Utah 84322.
[2] University of California, Los Alamos Scientific Laboratory, Los Alamos, New Mexico 87545.
[3] University of Texas at Dallas, Richardson, Texas 75080.
[4] NASA Goddard Space Flight Center, Greenbelt, Maryland 20771.
[5] Geophysical Institute, University of Alaska, College, Alaska 99701.

Paper number 6A0690.

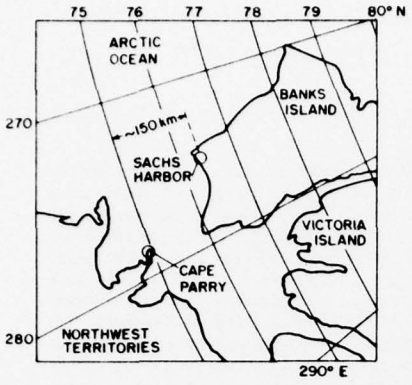

Fig. 1. Rockets were launched from Cape Parry, Northwest Territories, Canada. Ionosondes were located at Cape Parry and Sachs Harbor. Coordinates are invariant geomagnetic latitude and longitude [*Evans et al.*, 1969] at an altitude of 300 km.

IMF measurements were obtained by Imp 8. The discussion below will be limited to ionograms made on those days.

We first examine two sequences of ionograms to give the reader an idea of the type of data upon which the conclusions below are based. These sequences are intended to emphasize the rapid and dramatic variations that can occur in the ionograms and to indicate the problems that may arise when one tries to deduce the position of the cleft.

The first sequence (Figure 2) was made on December 6, 1974, from 2305 to 2325 UT. (The rocket flight described by *Shepherd et al.* [1976] began at 2332:06 UT.) The Sachs Harbor records do not show much change throughout this period. There is some evidence of the normal *X* and *O F* layer traces, but the critical frequencies are not particularly well defined (except at 2315, where the second-order trace is fairly clean). Throughout most of the records there is an irregular feature extending past 5 MHz between 300 and 400 km that shows

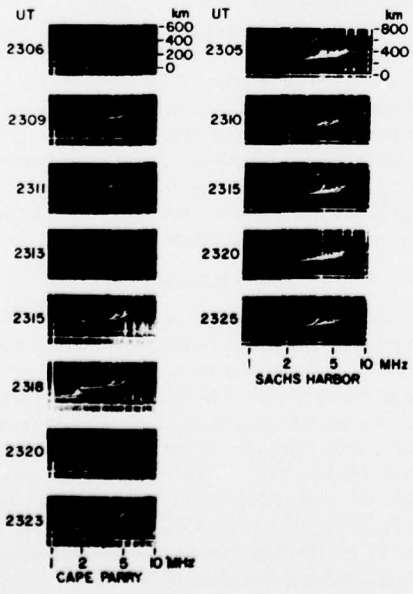

Fig. 2. Ionograms from Cape Parry and Sachs Harbor for December 6, 1974.

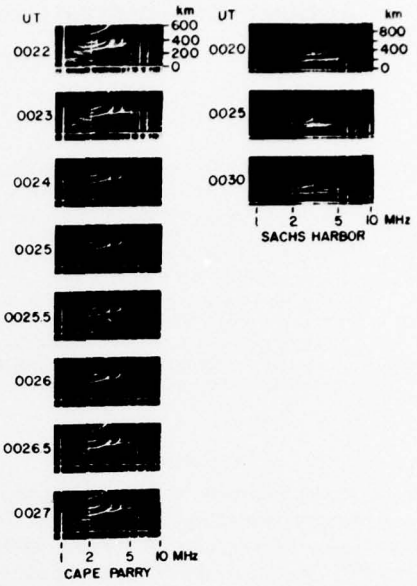

Fig. 3. Ionograms for January 11, 1975.

spreading and only a small amount of retardation at its high-frequency end. Such irregularities are characteristic of the cleft and, with the presence of the obscured *X* and *O* traces, suggest that the equatorward boundary of the cleft is located close to Sachs Harbor.

The Cape Parry records differ greatly from those made at Sachs Harbor. At 2306 the Cape Parry *O* and *X* traces are better defined. At this time the only evidence of the cleft at Cape Parry is several horizontal features just above 5 MHz between about 390 and 510 km. As is explained in the work by *Pike* [1971, 1972], these returns are interpreted as being oblique reflections from ionospheric features that are not directly above the sounder. The closest feature is presumed to be the equatorward edge of the cleft precipitation zone. The measured height (~390 km for the closest feature) thus gives the slant range along the oblique path to the edge of the cleft. The actual altitude of the cleft must be assumed. Note that at 2306, virtually no returns are visible between 300 and 400 km from ~2 to ~3.5 MHz.

In the next ionogram (2309 UT), however, there is a strong oblique return (with retardation at its high- and low-frequency ends) from the cleft between 2 and 5 MHz with a minimum range of ~360 km. It does not appear that this feature is the result of a simple equatorward motion of the cleft; the feature at 430 km (3.5 MHz) at 2306 actually seems to have moved poleward (to ~450 km) by 2309.

By 2311 there is a strong cleft return at ~315 km. There is a hint of a return near this altitude at 2309, and it is not clear whether the strong return at 2309 has moved equatorward or whether a new feature has appeared. The short feature at ~3.4 MHz, ~350 km may be the remains of the strong trace at 2309.

Throughout the remainder of the sequence the ionograms continue to show rapid variations. At times there may be only one predominant trace (2313, 300 km, 3 MHz, and 2320, 340 km, 3 MHz), while minutes later several weaker cleft returns may be detectable (2315 and 2323). (Note that the appearance of a strong sharp return at short range seems to preclude observation of weaker returns at longer ranges.) The virtual

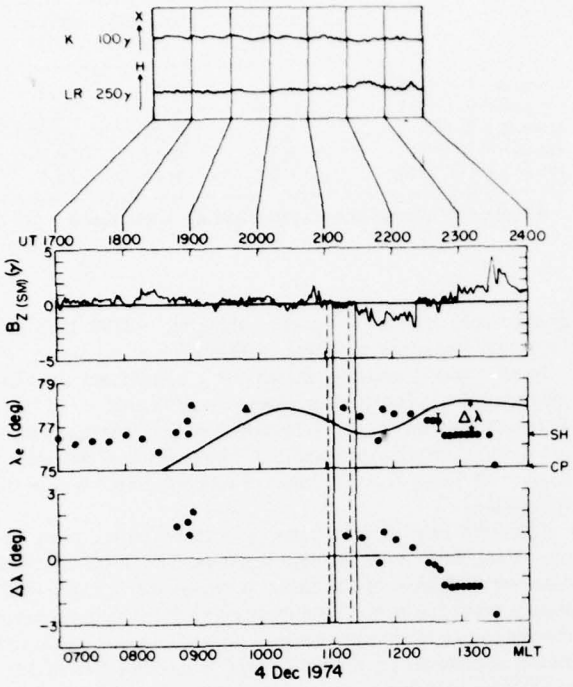

Fig. 4. Ground magnetograms, interplanetary magnetic field, and invariant latitude of the cleft for December 4, 1974. See text for explanation. Magnetic local time is shown along the bottom.

heights of the returns may vary by several tens of kilometers from record to record. It is difficult to account for these changes in height and appearance by assuming that the cleft as a whole is simply moving latitudinally.

The second sequence of ionograms (Figure 3) was made just prior to the second LASL-UAK barium release, which occurred at 0032 UT on January 11, 1975. As in Figure 2 the Sachs Harbor records indicate that the equatorward edge of the cleft is very close and possibly overhead. The *F* layer (*X* and *O*) traces show considerable frequency spreading. At 0020 a broad trace extending from about 2.7 MHz at 200 km to about 5.7 MHz at 230 km may be seen; this may be an auroral *E* layer seen obliquely. Five minutes later this feature has increased about 30 km in range. Note that the space between 200 and 300 km is almost filled at 3 MHz. At 0030 there are two strong traces, one like the first feature at 0020 at 200 km and another cleftlike trace near 260 km. A fainter trace may be seen near 350 km.

The Cape Parry records in this interval show, as in the previous example, more variation than do those from Sachs Harbor. Throughout the sequence the *X* and *O* returns from the normal *F* layer may be seen. The traces at ~300 and ~350

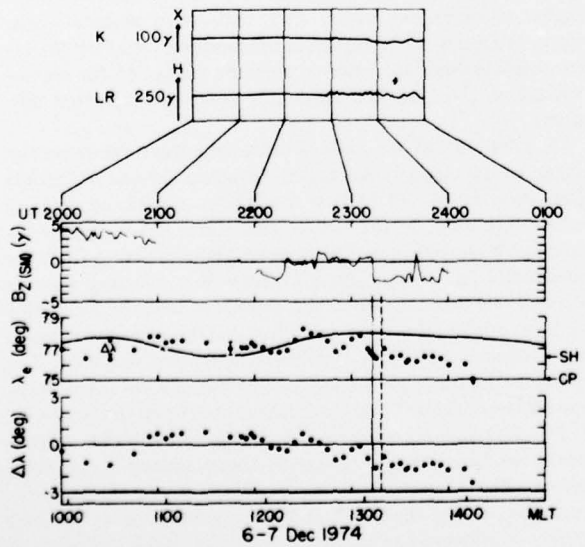

Fig. 5. December 6-7, 1974.

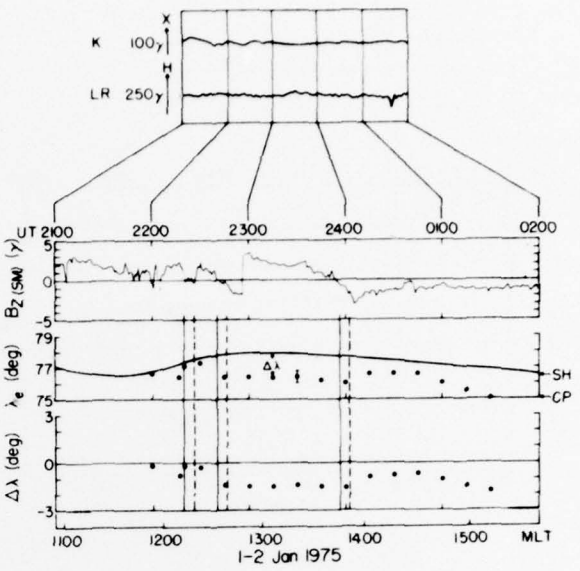

Fig. 6. January 1-2, 1975.

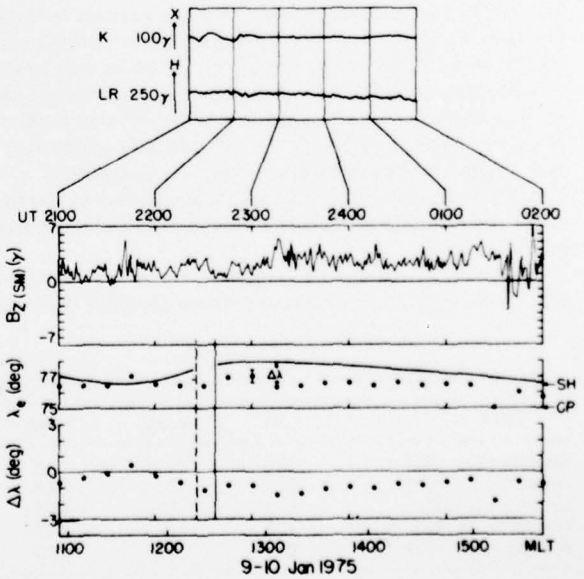

Fig. 7. January 9-10, 1975.

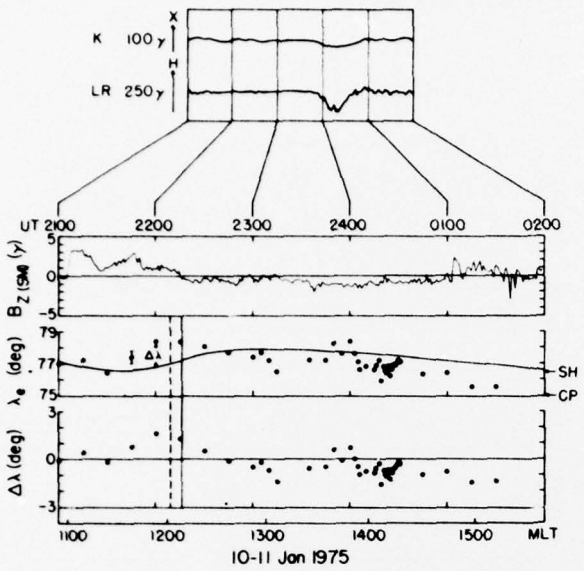

Fig. 8. January 10–11, 1975.

km between 1.5 and 2.5 MHz, which show the same shape as the *O* trace, are probably returns from a tilted *F* layer poleward of the station and in the vicinity of the equatorward edge of the cleft.

The cleft returns in this sequence may be found between ~300 and ~500 km at frequencies above (to the right of) the *X* trace. At 0022 two cleft returns may be seen at 300 and 340 km. Over the next 5 min these returns change rapidly. It appears that all the traces may be drifting poleward at a rate (~0.5 km/s) sufficient to produce an increase in slant range of ~20 km/min. Drifts of similar magnitude and direction have been reported for the *F* layer plasma in the cleft [*Knudsen*, 1974] and dayside auroral features [*Vorobjev et al.*, 1975]. Note again that at several times, multiple cleftlike returns can be seen.

Before proceeding with the discussion of the analysis of ionograms of this type we should summarize briefly their more important characteristics. First, as is most obvious from the examples, the appearance of the ionograms may change significantly on a time scale of a minute or so; traces may appear and disappear rapidly. Second, the ionograms from the two stations may differ greatly (this is due to the different positions of the two stations relative to the cleft and may reflect significant changes in the nature of the cleft over distances of ~100 km). These factors greatly complicate the process of tracking the cleft by simply measuring the slant range of apparently oblique returns.

The results of scaling the ionograms are shown in Figures 4–8. At the top of each figure are shown nightside magneto-

TABLE 1. Position of Imp 8 in Solar Magnetospheric Coordinates

Date	r, R_E	ϕ, deg	θ, deg
December 4–5, 1974	33.6	303.2	6.4
December 6–7, 1974	27.6	21.3	42.9
January 1–2, 1975	31.2	93.4	15.1
January 9–10, 1975	33.2	259.1	−14.2
January 10–11, 1975	28.5	287.1	9.7

TABLE 2. College *K* and Planetary *Kp* Magnetic Activity Indices

Date	1800–2100 UT	2100–2400 UT	0000–0300 UT
December 4–5, 1974	1, 1	1, 1	1, 1
December 6–7, 1974	0, 0+	0, 1−	0, 2−
January 1–2, 1975	1, 2	1, 2−	0, 1+
January 9–10, 1975	1, 1−	0, 1+	0, 2−
January 10–11, 1975	1, 0+	0, 1+	0, 2

K is the first number in each entry, and *Kp* is the second.

grams from Kiruna (magnetic midnight, ~2100 UT) and Leirvogur (magnetic midnight, ~0000 UT).

In the second panel is shown the z component (in solar magnetospheric coordinates, positive northward) of the IMF. These measurements are 1.02-min averages. The data show occasional gaps of several minutes. The position of the satellite is given in Table 1. At all times of interest, Imp 8 was in the solar wind.

The solid vertical lines drawn across the panels mark approximate times when B_z goes negative. The dashed vertical lines are estimates of the times at which the changes in B_z should reach the nose of the magnetosphere if the associated change in the total field vector is primarily a latitudinal one and at approximately the fixed longitudinal direction of 135° (or 315°) and if this discontinuity (or gradient) moves radially outward from the sun at ~ 450 km/s. (The longitudinal direction and the solar wind speed have been checked against the available data and faithfully apply to most events within acceptable error limits.) Since we are limited to data from one satellite, we obviously cannot determine with certainty the surface of the change in B_z; the dashed lines are intended only as rough estimates.

The third panel gives the absolute location λ_c in corrected geomagnetic latitude of the equatorward edge of the cleft as determined by the method described below. The fourth panel gives the deviation $\Delta\lambda$ of the cleft from its expected position. The expected position, which is a function of magnetic local time, is a smoothed version of the results of *Winningham* [1972] and is shown as a solid line in the third panel. It may be that Winningham's curve should be shifted a degree or so to higher latitudes [see *Burch*, 1972] because of seasonal variations. We are more interested in the motion of the cleft than in its absolute position, however, and the correction for diurnal variations given by Winningham's curve is considered adequate.

The latitude of the cleft is calculated from the measured range of the closest echo and an assumed altitude of 260 km [see *Pike et al.*, 1974]. All ionograms containing oblique echoes are used. In the initial calculations a flat earth is assumed for convenience. The distance along the earth from the ionosonde to a point directly below the reflecting layer is derived and then translated into degrees of latitude. This value is then added to the invariant latitude of the ionosonde to give the location of the equatorward boundary of the cleft. The invariant latitudes of the ionosonde stations are taken from the 300-km altitude values of *Evans et al.* [1969] (see Figure 1).

For the relatively small ranges of latitude involved (~4°) the use of the flat earth approximation does not result in very large errors. The correction to the position of the cleft's lower boundary is less than 0.1° and approaches zero as the cleft moves southward toward the ionosondes. Since this error is

about a factor of 4 smaller than that introduced by the uncertainties in the measurements of the slant ranges, it has not been corrected in the final results. Uncertainties of ±10 km in the slant range and assumed altitude yield a spread of about ±0.4° in the latitude.

During the December period of observation, periodic measurements of the cleft location were also made by the Isis 2 satellite. The satellite measurements are shown by solid triangles in the plots of λ_e for December 4 and December 6. Absorption prevented ionosonde measurements at the time of the December 4 satellite crossing. Simultaneous measurements were obtained on December 6 and on another day later in the month when IMF data were not available. On these two occasions the ionosonde and satellite measurements of the cleft's position agreed to within 0.5°.

Magnetic conditions during the observations are shown in Table 2. The local *K* for College, a station near the magnetic longitude of the ionosondes, is shown as well as the planetary index *Kp*.

December 4, 1974

As is true throughout most of the periods to be covered, this time was fairly quite magnetically (Figure 4). The College magnetogram showed a small amount of activity at 2020, 2130, and 2350. Small positive bays (~50 γ) were recorded at Leirvogur from 2220 to 2250 and at 2340.

The *z* component of the IMF shows small fluctuations throughout the period; these fluctuations are probably due to waves propagating upstream from the bow shock [*Heppner et al.*, 1967]. B_z is mostly positive, but does turn significantly negative from 2128 to 2222 UT.

The cleft measurements are unfortunately prevented by *D* region absorption of the ionosonde signals from 1900 and 2100. Just prior to 1900, Δλ is between +1° and +2°. The cleft remains mostly poleward of its expected position until ~2200, when it begins to move equatorward. This motion continues until about 2240, when the equatorward edge comes to rest over Sachs Harbor. Equatorward motion resumes at 2330, and for the remainder of the period the equatorward edge was at least as far south as Cape Parry.

Because of the gap caused by the absorption it is difficult to associate with certainty the equatorward motion of the cleft at 2200 with the southward turning of B_z at 2128. The sudden equatorward movement of the cleft at 2330 is quite clear, however, and coincides (within the resolution available) with the onset of the small positive bay at Leirvogur.

December 6–7, 1974

At the time at which the IMF measurements begin, B_z is northward at about +4 γ and is slowly decreasing (Figure 5). Unfortunately, there is a large gap in the IMF data between 2100 and 2200. It is thus not possible to determine exactly when B_z first becomes negative.

The cleft first begins to move equatorward at about 2200 UT, possibly soon after B_z goes negative. This motion continues until about 2215, when both Δλ and B_z become more positive. B_z remains close to zero until 2313, when it turns sharply southward. During this time the cleft first moves poleward, peaking at ~2230, then moves equatorward until ~2250, and then moves poleward until 2309, when it moves sharply equatorward.

Because of the gap in the magnetic data it is not possible to establish the timing between the initial equatorward motion of the cleft at 2200 and the southward turning of the field. Nor is it clear why Δλ goes negative again after 2230. It may be that the motion of the cleft from 2200 to 2305 is related to oscillations in the position of the magnetopause, such as have been reported by, for example, *Aubry et al.* [1970] and derived theoretically by *Holzer and Reid* [1975]. The period in the present case (~30 min) is longer by a factor of 2 or more than the reported periods, however.

The drop in Δλ at 2309 may be associated with the sharp change in B_z at 2313. Allowing for the assumed propagation delay, Δλ thus drops about 10 min before the change in B_z. The inconsistency may be due to the fact that the satellite was ~18 R_E above the ecliptic plane and that the discontinuity was in a plane other than that assumed. These circumstances may invalidate our simple model for the propagation of changes in B_z. Following this drop the cleft remains about 1.5° below its expected position and does not return poleward as it did following the decrease of 2200. This difference might be accounted for by the fact that B_z remains significantly southward after 2313, while it became more positive following the decrease at 2200.

Since the geomagnetic activity is so low prior to 2345, we assume that the motion of the cleft up to this time is due principally to changes in the IMF. On the other hand, from 2345 on, B_z remains southward, and one would not expect it to be responsible for the equatorward motion of the cleft at 0015. This motion may be associated with the weak geomagnetic activity from ~2400 on.

January 1–2, 1975

B_z is relatively smooth on this day and exhibits three well-defined southward turnings, one sharp drop at 2220 and two significant zero crossings at ~2242 and 2355 (Figure 6). The nightside magnetograms are again very quiet, but Leirvogur did record a sharp negative bay of < 100 γ beginning at 0135.

Although there is little magnetic activity and B_z is northward until ~2240, the cleft is found equatorward of its expected position throughout the period. The sharp drop in B_z near 2220 does not appear to provoke a response in λ_e, possibly because B_z does not go very negative or because the cleft is already somewhat equatorward. The cleft does move equatorward at 2245, about 5 min after the southward turning of B_z. B_z returns to positive values within several minutes, but Δλ remains at about −1.5° for the ensuing hour. Why Δλ stays depressed is not clear; there is only a very small amount of magnetic activity ($\Delta H < 50$ γ) recorded on the nightside at this time.

When B_z becomes negative again at 2355, Δλ actually becomes more positive, in contrast to the earlier results. B_z remains near −1 γ throughout the rest of the period, but the cleft begins to move equatorward again at 0100. The cause of this motion is also unclear; it may be simply an extreme example of the diurnal motion.

January 9–10, 1975

During this interval, B_z again shows evidence of upstream waves and does not exhibit any well-defined sustained changes in direction (Figure 7). B_z is positive throughout most of the record. Aside from some small disturbances from ~2100 to ~2230, nightside magnetic activity is quiet.

During the first hour the cleft is moving poleward. At 2200, Δλ starts to become more negative, possibly in response to the geomagnetic activity occurring at that time. For the remainder of the period the cleft remains a degree or so equatorward of its expected position.

January 10–11, 1975

B_z is somewhat erratic but shows a fairly clean change in direction from northward to southward at about 2216 (Figure 8). Note that there is a sharp jump in B_z at 2105; the College magnetogram also shows a jump in H at the same time. Such changes in high-latitude magnetic records are often correlated with changes in the IMF [*Burch*, 1972]. This indicates that there may be little propagation delay for the solar wind between Imp 8 and the front of the magnetosphere.

Leirvogur recorded a substorm beginning at about 2350; the negative bay peaked at ~ -130 γ at 0020 and recovered by 0050. Small (<50 γ) fluctuations followed for the next hour. (Note that Leirvogur also detected the small jump at $\sim$2105.)

Prior to 2200, while $B_z > 0$, the cleft is seen to be moving generally poleward. At 2215, close to the southward turning of B_z, the cleft begins to move equatorward. This motion continues for about another hour. The average rate of the motion until 2315, when the cleft appears to reach an equilibrium, is about 0.04°/min.

From 2330 to 2400 the cleft appears to be drifting poleward again. At about 2400, just after the onset of the negative bay at Leirvogur, the cleft rapidly moves about 2° equatorward. For the remainder of the observation, $\Delta\lambda$ remains negative, even though B_z becomes more positive after 0100.

Summary

There are eleven cases when the edge of the cleft shows significant equatorward motion. In agreement with the earlier work mentioned in the introduction it appears that the cleft responds both to changes in the polarity of B_z (four cases: 2200 and 2313 December 6, 2245 January 1, and 2216 January 10) and to the occurrence of geomagnetic disturbances (two cases: 2332 December 4 and 2400 January 10). In 2 of the 11 cases the motion of the cleft did not appear to be associated with either B_z or a magnetic disturbance (2230 December 6 and 0100 January 2). In the remaining cases (2200 December 4, 0015 December 7, and 2200 January 9) several factors precluded forming even tentative conclusions.

In examining eight cases where the cleft moves poleward we find only two (2215 December 6 and 2130 January 10) that may be associated with B_z becoming more positive. Three events occur when B_z does not show any clear change (2250 December 6, 2100–2140 January 9, and 2330–2400 January 10). The January 10 event, which occurs while B_z is negative, may be associated with the onset of a negative bay; there is also a small amount of geomagnetic activity on January 9. The remaining three cases occur either while B_z is positive and decreasing (1900 December 4 and 2030 December 6) or when it has turned southward (2400 January 1).

The cleft appears to respond fairly rapidly to changes in the IMF. The records of December 6–7, January 1–2, and particularly January 10–11 indicate that the cleft may begin to move equatorward within 10 min or less of the time when the change in B_z reaches the front of the magnetosphere.

The velocity of the equatorward motion, once it begins varies significantly. On December 6–7 and January 1–2 the cleft moved equatorward at about 0.5°/min. On December 4 and January 10–11 the rate was less than 0.1°/min.

The duration of the motion also varied. When the motion was faster (December 6–7 and January 1–2), it ceased after about 15 min. In those cases of slower motion (December 4 and January 10–11) it continued for about an hour. The total change $\Delta\lambda$ for a single event varies from 1 to 3 deg.

The temporal relation between geomagnetic activity and the cleft's motion is less clear. The records suggest, however, that the cleft begins to move within 10 min or so of the onset of activity. On January 10–11, for example, the negative bay appeared at 2350, and the equatorward motion began at 2402.

DISCUSSION

In the previous section we found evidence that the cleft may at times move equatorward in response to a southward turning of the z component of the IMF and to the occurrence of geomagnetic disturbances. These events agree with the conclusions of earlier work. *Burch* [1972, 1973] analyzed Ogo 4 particle measurements and found that the equatorward boundary of cleftlike precipitation moves to lower latitudes by several degrees during substorms and/or in the presence of negative B_z. *Pike et al.* [1974] monitored the cleft with an airborne ionosonde and found that the cleft typically moved equatorward following a southward turning of B_z. Recently, *Kamide et al.* [1976], combining the Ogo 4 and the Isis 1 data, also found a tendency for the cleft to move equatorward with southward B_z and the occurrence of substorms.

It is important to note that we also found several examples where the motion of the cleft does not correspond to these results. The earlier investigations do provide convincing evidence that on the average, the cleft moves equatorward in response to increasing geomagnetic activity and southward B_z. These conclusions are based largely upon satellite data, however, which provide no more than roughly one measurement of the cleft's position per hour; the conclusions may not hold on a time scale of several minutes.

In the only previous work [*Pike et al.*, 1974] in which the relation between B_z and the cleft's position was studied with high time resolution, it was concluded that the cleft responds to changes in B_z after a delay of about 15 min. Our results suggest that when the cleft does respond, the delay may be as short as $\sim$10 min

Burch [1972] gives an estimate of the rate at which the cleft moves equatorward following a southward turning of B_z. His value of $\sim$0.1°/min is based upon a single measurement of the cleft's position during each event (necessitated by the fact that the data were taken by satellite). In this study, where the measurements are ground based and may be made several times during each event, we have found that the cleft may move equatorward as rapidly as $\sim$0.5°/min. However, the rate of motion may fall as low as $\sim$0.05°/min.

One of the goals of earlier efforts has been to obtain a quantitative relation between the cleft's location and B_z. *Burch* [1973], for example, derives from his data an expression for the position of the cleft as a function of the average value of B_z over the previous 45 min. Such an expression may agree fairly well with the average behavior of the cleft and those instances where the cleft moves equatorward fairly slowly in response to a southward turning. Since a 45-min average of B_z is used, however, the expression will not be able to account for those cases where the cleft moves a degree or two in only a few minutes (e.g., December 6–7 and January 10–11). Nor will the expression account for those times when the movement of the cleft and B_z appear to be unrelated.

The variation in the response of the cleft implies that any scheme for predicting the cleft's position based upon a fixed length average of B_z will not be accurate at all times. It is important to note that any theoretical description of the mechanism linking the IMF and the position of the cleft must be able to account for such variations. Such a description will apparently have to include other factors, including geomag-

netic conditions [*Kamide et al.*, 1976] and perhaps the state of the ionosphere [*Holzer and Reid*, 1975].

CONCLUSIONS AND SUGGESTIONS

We have reported the results of the analysis of 5 days of ionogram data from two stations located in northern auroral latitudes. The ionospheric manifestation of the cleft has been found to be very complex and dynamic. The returns frequently show considerable structure and may change significantly in just a minute or two.

A clear relation between the position of the cleft and the IMF (or geomagnetic activity) has not emerged from the study of this small sample. Events have been found which agree with earlier conclusions that southward turnings of B_z and geomagnetic activity are associated with equatorward motion of the cleft. Other events, however, indicate that at times the motion may be contrary to that expected and may depend on other causes.

The results do suggest that a program of taking ionograms in high time resolution (spacing, $\lesssim$1 min) would improve our knowledge of the factors that control the cleft's position. The cleft has been found to change rapidly, and it may be that the key to its behavior will be found only when these rapid changes are better understood.

Acknowledgments. The LASL portion of this work was performed under the auspices of the U.S. Energy Research and Development Administration (ERDA). The University of Texas at Dallas portion of this work was supported by ERDA contracts KH-69046-1 and LC5-83449-1, Air Force Cambridge Research Laboratories contracts F19628-75-C-0032 and F19628-76-C-0005, and NASA contract NGR 44-004-124. University of Alaska operations were supported by NASA contract NGR02-001-087. The Kiruna and Leirvogur magnetograms were obtained through the World Data Center A for Solar Terrestrial Physics (geomagnetism). The authors thank the referees for their comments.

The Editor thanks J. A. Whalen and J. H. Whitteker for their assistance in evaluating this paper.

REFERENCES

Aubry, M. P., C. T. Russell, and M. G. Kivelson, On inward motion of the magnetopause during a substorm, *J. Geophys. Res.*, *75*, 7018, 1970.

Burch, J. L., Precipitation of low-energy electrons at high latitudes: Effects of interplanetary magnetic field and dipole tilt angle, *J. Geophys. Res.*, *77*, 6696, 1972.

Burch, J. L., Rate of erosion of dayside magnetic flux based on a quantitative study of the dependence of polar cusp latitude on the interplanetary magnetic field, *Radio Sci.*, *8*, 955, 1973.

Evans, J. E., L. L. Newkirk, and B. M. McCormac, North polar, south polar, world maps and tables of invariant magnetic coordinates for six altitudes: 0, 100, 300, 600, 1000, and 3000 km, *DASA 2347*, Lockheed Palo Alto Res. Lab., Palo Alto, Calif., 1969.

Frank, L. A., Plasma in the earth's polar magnetosphere, *J. Geophys. Res.*, *76*, 5202, 1971.

Frank, L. A., and K. L. Ackerson, Observations of charged particle precipitation into the auroral zone, *J. Geophys. Res.*, *76*, 3612, 1971.

Heikkila, W. J., and J. D. Winningham, Penetration of magnetosheath plasma to low altitudes through the dayside magnetospheric cusps, *J. Geophys. Res.*, *76*, 883, 1971.

Heikkila, W. J., J. B. Smith, J. Tarstrup, and J. D. Winningham, The soft particle spectrometer in the Isis 1 satellite, *Rev. Sci. Instrum.*, *41*, 1393, 1970.

Heppner, J. P., M. Sugiura, T. L. Skillman, B. G. Ledley, and M. Campbell, Ogo-A magnetic field observations, *J. Geophys. Res.*, *72*, 5417, 1967.

Holzer, T. E., and G. C. Reid, The response of the dayside magnetosphere-ionosphere system to time-varying field line reconnection at the magnetopause, 1, Theoretical model, *J. Geophys. Res.*, *80*, 2041, 1975.

Jeffries, R. A., W. H. Roach, E. W. Hones, Jr., E. M. Wescott, H. C. Stenbaek-Nielsen, T. N. Davis, and J. D. Winningham, Two barium plasma injections into the northern magnetospheric cleft, *Geophys. Res. Lett.*, *2*, 285, 1975.

Kamide, Y., J. L. Burch, J. D. Winningham, and S.-I. Akasofu, Dependence of the latitude of the cleft on the interplanetary magnetic field and substorm activity, *J. Geophys. Res.*, *81*, 698, 1976.

Knudsen, W. C., Magnetospheric convection and the high-latitude F_2 ionosphere, *J. Geophys. Res.*, *79*, 1046, 1974.

Pike, C. P., A latitudinal survey of the daytime polar *F* layer, *J. Geophys. Res.*, *76*, 7745, 1971.

Pike, C. P., Equatorward shift of the polar *F* layer irregularity zone as a function of the *Kp* index, *J. Geophys. Res.*, *77*, 6911, 1972.

Pike, C. P., and J. A. Whalen, Satellite observations of auroral substorms, *J. Geophys. Res.*, *79*, 985, 1974.

Pike, C. P., C.-I. Meng, S.-I. Akasofu, and J. A. Whalen, Observed correlations between interplanetary magnetic field variations and the dynamics of the auroral oval and the high-latitude ionosphere, *J. Geophys. Res.*, *79*, 5129, 1974.

Russell, C. T., C. R. Chappell, M. D. Montgomery, M. Neugebauer, and F. L. Scarf, Ogo 5 observations of the polar cusp on November 1, 1968, *J. Geophys. Res.*, *76*, 6743, 1971.

Shepherd, G. G., J. F. Pieau, F. Creutzberg, A. G. McNamara, J. C. Gerard, D. J. McEwen, B. Delana, and J. H. Whitteker, Rocket and ground-based measurements of the dayside magnetospheric cleft from Cape Parry, N.W.T., *Geophys. Res. Lett.*, *3*, 69, 1976.

Ungstrup, E., A. Bahnsen, J. K. Olesen, F. Primdahl, F. Spangslev, W. J. Heikkila, D. M. Klumpar, J. D. Winningham, U. Fahleson, C.-G. Falthammar, and A. Pedersen, Rocket-borne particle, field, and plasma observations in the cleft region, *Geophys. Res. Lett.*, *2*, 345, 1975.

Vasyliunas, V. M., Magnetospheric cleft symposium, *Eos Trans. AGU*, *55*, 60, 1974.

Vorobjev, V. G., G. Gustafsson, G. V. Starkov, Y. I. Feldstein, and N. F. Shevnina, *Planet. Space Sci.*, *23*, 269, 1975.

Whalen, J. A., and C. P. Pike, *F* layer and 6300-Å measurements in the day sector of the noon oval, *J. Geophys. Res.*, *78*, 3848, 1973.

Winningham, J. D., Penetration of magnetosheath plasma to low altitudes through the dayside magnetospheric cusps, Ph.D. dissertation, Tex. A&M Univ., College Station, 1970.

Winningham, J. D., Characteristics of magnetosheath plasma observed at low altitudes in the dayside magnetospheric cusps, in *Earth's Magnetospheric Processes*, edited by B. M. McCormac, p. 68, D. Reidel, Dordrecht, Netherlands, 1972.

Winningham, J. D., and C. P. Pike, In situ observations of the effects of magnetosheath particle precipitation on the dayside ionosphere (abstract), *Eos Trans. AGU*, *53*, 361, 1972.

(Received April 15, 1976;
accepted September 8, 1976.)